

1
2 **Heat stored in the Earth system: Where does the energy go?**
3 **The GCOS Earth heat inventory team**

4 Karina von Schuckmann¹, Lijing Cheng^{2,28}, Matthew D. Palmer³, James Hansen⁴, Caterina
5 Tassone⁵, Valentin Aich⁵, Susheel Adusumilli⁶, Hugo Beltrami⁷, Tim Boyer⁸, Francisco José
6 Cuesta-Valero^{7,27}, Damien Desbruyères⁹, Catia Domingues^{10,11}, Almudena García-García⁷, Pierre
7 Gentine¹², John Gilson¹³, Maximilian Gorfer¹⁴, Leopold Haimberger¹⁵, Masayoshi Ishii¹⁶, Gregory
8 C. Johnson¹⁷, Rachel Killick³, Brian A. King¹⁰, Gottfried Kirchengast¹⁴, Nicolas Kolodziejczyk¹⁸,
9 John Lyman¹⁷, Ben Marzeion¹⁹, Michael Mayer^{15,29}, Maeva Monier²⁰, Didier Paolo Monselesan²¹,
10 Sarah Purkey⁶, Dean Roemmich⁶, Axel Schweiger²², Sonia I. Seneviratne²³, Andrew Shepherd²⁴,
11 Donald A. Slater⁶, Andrea K. Steiner¹⁴, Fiammetta Straneo⁶, Mary-Louise Timmermans²⁵, Susan
12 E. Wijffels^{21,26}

13
14 ¹Mercator Ocean International, France

15 ²Institute of Atmospheric Physics, Chinese Academy of Sciences, China

16 ³Met Office Hadley Centre, UK

17 ⁴Columbia University Earth Institute, USA

18 ⁵WMO/GCOS, Switzerland

19 ⁶Scripps Institution of Oceanography, UCSD, San Diego, CA, USA

20 ⁷Climate & Atmospheric Sciences Institute, St. Francis Xavier University, NS, Canada

21 ⁸NOAA's National Centers for Environmental Information

22 ⁹Ifremer, University of Brest, CNRS, IRD, Laboratoire d'Océanographie Physique et Spatiale, France

23 ¹⁰National Oceanographic Centre, UK

24 ¹¹ARC Centre of Excellence for Climate Extremes, University of Tasmania, Hobart, Tasmania, Australia

25 ¹²Earth and Environmental Engineering in the School of Engineering and Applied Sciences, Columbia University,
26 USA

27 ¹³University of California, USA

28 ¹⁴Wegener Center for Climate and Global Change and Institute of Physics, University of Graz, Austria

29 ¹⁵Department of Meteorology and Geophysics, University of Vienna, Austria

30 ¹⁶Department of Atmosphere, Ocean and Earth System Modeling Research, Meteorological Research Institute, Japan

31 ¹⁷NOAA, Pacific Marine Environmental Laboratory, USA

32 ¹⁸University of Brest, CNRS, IRD, Ifremer, Laboratoire d'Océanographie Physique et Spatiale, IUEM, France

33 ¹⁹Institute of Geography and MARUM-Center for Marine Environmental Sciences, University of Bremen, Germany

34 ²⁰CELAD/Mercator Ocean International, France

35 ²¹CSIRO Oceans and Atmosphere, Hobart, Tasmania, Australia

36 ²²Polar Science Center, Applied Physics Laboratory, University of Washington, Seattle, USA

37 ²³Institute for Atmospheric and Climate Science, ETH, Switzerland

38 ²⁴Center for Polar Observation and Modeling, University of Leeds, UK

39 ²⁵Department of Earth and Planetary Sciences, Yale University, New Haven, USA

40 ²⁶Woods Hole Oceanographic Institution, Massachusetts, United States

41 ²⁷Environmental Sciences Program, Memorial University of Newfoundland, NL, Canada

42 ²⁸Center for Ocean Mega-Science, Chinese Academy of Sciences, Qingdao, China, 266071

43 ²⁹European Centre for Medium-Range Weather Forecasts, Reading, UK

44
45 *Correspondence to:* Karina von Schuckmann (karina.von.schuckmann@mercator-ocean.fr)

46
47
48
49
50
51
52
53
54
55
56
57
58
59
60
61
62
63
64
65
66
67
68
69
70
71
72
73
74
75
76
77
78
79
80
81
82
83
84

Abstract

Human-induced atmospheric composition changes cause a radiative imbalance at the top-of-atmosphere which is driving global warming. This Earth Energy Imbalance (EEI) is the most critical number defining the prospects for continued global warming and climate change. Understanding the heat gain of the Earth system – and particularly how much and where the heat is distributed – is fundamental to understanding how this affects warming ocean, atmosphere, and land; rising surface temperature; sea level; and loss of grounded and floating ice, which are fundamental concerns for society. This study is a Global Climate Observing System (GCOS) concerted international effort to update the Earth heat inventory, and presents an updated assessment of ocean warming estimates, and new and updated estimates of heat gain in the atmosphere, cryosphere and land over the period 1960-2018. The study obtains a consistent long-term Earth system heat gain over the period 1971-2018, with a total heat gain of 358 ± 37 ZJ, which is equivalent to a global heating rate of 0.47 ± 0.1 W/m². Over the period 1971-2018 (2010-2018), the majority of heat gain is reported for the global ocean with 89% (90%), with 52% for both periods in the upper 700m depth, 28% (30%) for the 700-2000m depth layer, and 9% (8%) below 2000m depth. Heat gain over land amounts to 6% (5%) over these periods, 4% (3%) is available for the melting of grounded and floating ice, and 1% (2%) for atmospheric warming. Our results also show that EEI is not only continuing, it is increasing: the EEI amounts to 0.87 ± 0.12 W/m² during 2010-2018. Stabilization of climate, the goal of the universally agreed UNFCCC in 1992 and the Paris agreement in 2015, requires that EEI be reduced to approximately zero to achieve Earth's system quasi-equilibrium. The amount of CO₂ in the atmosphere would need to be reduced from 410 ppm to 353 ppm to increase heat radiation to space by 0.87 W/m², bringing Earth back towards energy balance. This simple number, EEI, is the most fundamental metric that the scientific community and public must be aware of, as the measure of how well the world is doing in the task of bringing climate change under control, and we call for an implementation of the EEI into the global stocktake based on best available science. Continued quantification and reduced uncertainties in the Earth heat inventory can be best achieved through the maintenance of the current global climate observing system, its extension into areas of gaps in the sampling, as well as to establish an international framework for concerted multi-disciplinary research of the Earth heat inventory as presented in this study. This Earth heat inventory is published at DKRZ (<https://www.dkrz.de/>) under the doi: https://doi.org/10.26050/WDCC/GCOS_EHI_EXP_v2 (von Schuckmann et al., 2020).

85 Introduction

86

87 In the Paris Agreement of the United Nations Framework Convention on Climate Change
88 (UNFCCC), article 7 demands that “Parties should strengthen [...] scientific knowledge on
89 climate, including research, systematic observation of the climate system and early warning
90 systems, in a manner that informs climate services and supports decision-making.” This request of
91 the UNFCCC expresses the need of climate monitoring based on best available science, which is
92 globally coordinated through the Global Climate Observing System (GCOS). In the current
93 Implementation Plan of GCOS, main observation gaps are addressed and it states that “closing the
94 Earth's energy balance [...] through observations remain outstanding scientific issues that require
95 high-quality climate records of Essential Climate Variables (ECVs).” (GCOS, 2016). GCOS is
96 asking the broader scientific community to establish the observational requirements needed to
97 meet the targets defined in the GCOS Implementation Plan, and to identify how climate
98 observations could be enhanced and continued into the future in order to monitor the Earth’s cycles
99 and the global energy budget. This study addresses and intends to respond to this request.

100 The state, variability and change of Earth’s climate are to a large extent driven by the energy
101 transfer between the different components of the Earth system (Hansen, 2005; Hansen et al., 2011).
102 Energy flows alter clouds, and weather and internal climate modes can temporarily alter the energy
103 balance on sub-annual to multi-decadal timescales (Palmer & McNeall, 2014; Rhein et al., 2013).
104 The most practical way to monitor climate state, variability and change is to continually assess the
105 energy, mainly in the form of heat, in the Earth system (Hansen et al., 2011). All energy entering
106 or leaving the Earth climate system does so in the form of radiation at the top-of-the-atmosphere
107 (TOA) (Loeb et al., 2012). The difference between incoming solar radiation and outgoing
108 radiation, which is the sum of the reflected shortwave radiation and emitted longwave radiation,
109 determines the net radiative flux at TOA. Changes of this global radiation balance at TOA - the
110 so-called Earth Energy Imbalance (EEI) - determines the temporal evolution of Earth’s climate: If
111 the imbalance is positive (i.e. less energy going out than coming in), energy in the form of heat is
112 accumulated in the Earth system resulting in global warming - or cooling if the EEI is negative.
113 The various facets and impacts of observed climate change arise due to the EEI, which thus
114 represents a crucial measure of the rate of climate change (von Schuckmann et al., 2016). The EEI
115 is the portion of the forcing that has not yet been responded to (Hansen, 2005). In other words,
116 warming will continue even if atmospheric greenhouse gas (GHG) amounts are stabilized at
117 today’s level, and the EEI defines additional global warming that will occur without further change
118 in forcing (Hansen et al., 2017). The EEI is less subject to decadal variations associated with
119 internal climate variability than global surface temperature and therefore represents a robust
120 measure of the rate of climate change (von Schuckmann et al., 2016; Cheng et al., 2017).

121

122 The Earth system responds to an imposed radiative forcing through a number of feedbacks, which
123 operate on various different timescales. Conceptually, the relationships between EEI, radiative
124 forcing, and surface temperature change can be expressed as (Gregory & Andrews, 2016):

125

$$126 \quad \Delta N_{TOA} = \Delta F_{ERF} - |\alpha_{FP}| \Delta T_S \quad (1)$$

127
128 where ΔN_{TOA} is Earth's net energy imbalance at the Top of the Atmosphere (TOA, in $W m^{-2}$),
129 ΔF_{ERF} is the effective radiative forcing ($W m^{-2}$), ΔT_S is the global surface temperature anomaly
130 (K) relative to the equilibrium state, and α_{FP} is the net total feedback parameter ($W m^{-2} K^{-1}$), which
131 represents the combined effect of the various climate feedbacks. Essentially, α_{FP} in Equ. (1) can
132 be viewed as a measure of how efficient the system is at restoring radiative equilibrium for a unit
133 surface temperature rise. Thus, ΔN_{TOA} represents the difference between the applied radiative
134 forcing and Earth's radiative response through climate feedbacks associated with surface
135 temperature rise (e.g. Hansen et al., 2011). Observation-based estimates of ΔN_{TOA} are therefore
136 crucial both to our understanding of past climate change and for refining projections of future
137 climate change (Gregory & Andrews, 2016; Kuhlbrodt & Gregory, 2012). The long atmospheric
138 lifetime of carbon dioxide means that ΔN_{TOA} , ΔF_{ERF} and ΔT_S will remain positive for centuries,
139 even with substantial reductions in greenhouse gas emissions and lead to substantial committed
140 sea-level rise (Cheng, Abraham, et al., 2019; Hansen et al., 2017; Nauels et al., 2017; Matthew D
141 Palmer et al., 2018).

142
143 However, this conceptual picture is complicated by the presence of unforced internal variability in
144 the climate system, which adds substantial noise to the real-world expression of this equation
145 (Gregory et al., 2020; Marvel et al., 2018; Palmer & McNeall, 2014). For example, at time scales
146 from interannual to decadal periods, the phase of the El Niño Southern Oscillation contributes to
147 both positive or negative variations in EEI (Cheng, Trenberth, et al., 2019; Loeb et al., 2018;
148 Johnson and Birnbaum, 2017; Loeb et al., 2012). At multi-decadal and longer time scales,
149 systematic changes in ocean circulation can significantly alter the EEI as well (Baggenstos et al.,
150 2019).

151
152 Time-scales of the Earth climate response to perturbations of the equilibrium Earth energy balance
153 at TOA are driven by a combination of climate forcing and the planet's thermal inertia: The Earth
154 system tries to restore radiative equilibrium through increased thermal radiation to space via the
155 Planck response, but a number of additional Earth system feedbacks also influence the planetary
156 radiative response (Lembo et al., 2019; Myhre et al., 2013). Time-scales of warming or cooling of
157 the climate depend on the imposed radiative forcing, the evolution of climate and Earth system
158 feedbacks with ocean and cryosphere in particular leading to substantial "thermal inertia" (Clark
159 et al., 2016; Marshall et al., 2015). Consequently, it requires centuries for Earth's surface
160 temperature to respond fully to a climate forcing.

161
162 Contemporary estimates of the magnitude of the Earth's energy imbalance range between about
163 $0.4-0.9 W m^{-2}$ (depending on estimate method and period, see also conclusion), and are directly
164 attributable to increases in carbon dioxide and other greenhouse gases in the atmosphere from
165 human activities (Ciais et al., 2013, Myhre et al., 2013, Rhein et al., 2013, Hansen et al., 2011).
166 The estimate obtained from climate models (CMIP6) as presented by (Wild, 2020) amounts to 1.1

167 $\pm 0.8 \text{ W m}^{-2}$. Since the period of industrialization, the EEI has become increasingly dominated by
168 the emissions of radiatively active greenhouse gases, which perturb the planetary radiation budget
169 and result in a positive EEI. As a consequence, excess heat is accumulated in the Earth system,
170 which is driving global warming (Hansen et al., 2005; 2011). The majority (about 90%) of this
171 positive EEI is stored in the ocean (Rhein et al., 2013) and can be estimated through the evaluation
172 of ocean heat content (OHC, e.g. Abraham et al., 2013). According to previous estimates, a small
173 proportion ($\sim 3\%$) contributes to the melting of Arctic sea ice and land ice (glaciers, the Greenland
174 and Antarctic ice sheets). Another 4% goes into heating of the land and atmosphere (Rhein et al.,
175 2013).

176
177 Knowing where and how much heat is stored in the different Earth system components from a
178 positive EEI, and quantifying the Earth heat inventory is of fundamental importance to unravel the
179 current status of climate change, as well as to better understand and predict its implications, and
180 to design the optimal observing networks for monitoring the Earth heat inventory. Quantifying this
181 energy gain is essential for understanding the response of the climate system to radiative forcing,
182 and hence to reduce uncertainties in climate predictions. The rate of ocean heat gain is a key
183 component for the quantification of the EEI, and the observed surface warming has been used to
184 estimate the equilibrium climate sensitivity (e.g. Knutti & Rugenstein, 2015). However, further
185 insight into the Earth heat inventory, particularly to further unravel on where the heat is going, can
186 have implications on the understanding of the transient climate responses to climate change, and
187 consequently reduces uncertainties in climate predictions (Hansen et al., 2011). In this paper, we
188 focus on the inventory of heat stored in the Earth system. The first four sections will introduce the
189 current status of estimate of heat storage change in the ocean, atmosphere, land and cryosphere,
190 respectively. Uncertainties, current achieved accuracy, challenges, and recommendations for
191 future improved estimates are discussed for each Earth system component, and in the conclusion.
192 In the last chapter, an update of the Earth heat inventory is established based on the results of
193 sections 1-4, followed by a conclusion.

194

195

196 **1. Heat stored in the ocean**

197

198 The storage of heat in the ocean leads to ocean warming (IPCC, 2019), and is a major contributor
199 to sea-level rise through thermal expansion (WCRP, 2018). Ocean warming alters ocean
200 stratification and ocean mixing processes (Bindoff et al., 2019), affects ocean currents (Hoegh-
201 Guldborg, 2018; Monika Rhein et al., 2018; Yang et al., 2016), impacts tropical cyclones (Hoegh-
202 Guldborg, 2018; Trenberth et al., 2018; Woollings et al., 2012) and is a major player in ocean
203 deoxygenation processes (Breitburg et al., 2018) and carbon sequestration into the ocean (Bopp et
204 al., 2013; Frölicher et al., 2018). Together with ocean acidification and deoxygenation, ocean
205 warming can lead to dramatic changes in ecosystems, biodiversity, population extinctions, coral
206 bleaching and infectious disease, as well as redistribution of habitat (García Molinos et al., 2016;

207 Gattuso et al., 2015; Ramírez et al., 2017). Implications of ocean warming are also widespread
208 across Earth's cryosphere (Jacobs et al., 2002; Mayer et al., 2019; Polyakov et al., 2017; Serreze
209 & Barry, 2011; Shi et al., 2018). Examples include the basal melt of ice shelves (Adusumilli et al.,
210 2019; Pritchard et al., 2012; Wilson et al., 2017) and marine terminating glaciers (Straneo &
211 Cenedese, 2015); the retreat and speedup of outlet glaciers in Greenland (King et al., 2018) and in
212 Antarctica (Shepherd, Fricker, et al., 2018) and of tidewater glaciers in South America and in the
213 High Arctic (Gardner et al., 2013).

214
215 Opportunities and challenges in forming OHC estimates depend on the availability of in situ
216 subsurface temperature measurements, particularly for global-scale evaluations. Subsurface ocean
217 temperature measurements before 1900 had been obtained from ship-board instrumentation,
218 culminating in the global-scale Challenger expedition (1873–1876) (Roemmich & Gilson, 2009).
219 From 1900 up to the mid-1960s, subsurface temperature measurements relied on ship-board
220 Nansen-Bottle and mechanical bathythermograph (MBT) instruments (Abraham et al., 2013), only
221 allowing limited global coverage and data quality. The inventions of the conductivity-temperature-
222 depth (CTD) instruments in the mid-50s and the Expendable Bathythermograph Observing (XBT)
223 system about ten years later increased the oceanographic capabilities for widespread and accurate
224 (in the case of the CTD) measurements of in situ subsurface water temperature (Abraham et al.,
225 2013; Goni et al., 2019).

226
227 With the implementation of several national and international programs, and the implementation
228 of the moored arrays in the tropical ocean in the 1980s, the Global Ocean Observing System
229 (GOOS, <https://www.goosoocean.org/>) started to grow. Particularly the global World Ocean
230 Circulation program (WOCE) during the 1990s obtained a global baseline survey of the ocean
231 from top-to-bottom (King et al., 2001). However, measurements were still limited to fixed point
232 platforms, major shipping routes and Naval and research vessel cruise tracks, leaving large parts
233 of the ocean under-sampled. In addition, detected instrumental biases in MBTs, XBTs and other
234 instruments pose a further challenge for the global scale OHC estimate (Abraham et al., 2013;
235 Ciais et al., 2013; M. Rhein et al., 2013), but significant progress has been made recently to correct
236 biases and provide high-quality data for climate research (Boyer et al., 2016; Cheng et al., 2016;
237 Goni et al., 2019; Gouretski & Cheng, 2020). Satellite altimeter measurements of sea surface
238 height began in 1992, and are used to complement in situ derived OHC estimates, either for
239 validation purposes (Cabanes et al., 2013), or to complement the development of global gridded
240 ocean temperature fields (Guinehut et al., 2012; Willis et al., 2004). Indirect estimates of OHC
241 from remote sensing through the global sea level budget became possible with satellite-derived
242 ocean mass information in 2002 (Dieng et al., 2017; Llovel et al., 2014; Loeb et al., 2012;
243 Meyssignac et al., 2019; von Schuckmann et al., 2014).

244
245 After the Oceanobs conference in 1999, the international Argo profiling float program was
246 launched with first Argo float deployments in the same year (Riser et al., 2016; Roemmich &

247 Gilson, 2009). By the end of 2006, Argo sampling had reached its initial target of data sampling
248 roughly every 3 degrees between 60°S-60°N. However, due to technical evolution, only 40% of
249 Argo floats provided measurements down to 2000 m depth in the year 2005, but that percentage
250 increased to 60% in 2010 (von Schuckmann & Le Traon, 2011). The starting point of Argo-based
251 ‘best estimate’ for near-global-scale (60°S-60°N) OHC is either defined in 2005 (von Schuckmann
252 and Le Traon, 2011), or in 2006 (Wijffels et al., 2016). The opportunity for improved OHC
253 estimation provided by Argo is tremendous, and has led to major advancements in climate science,
254 particularly on the discussion of the EEI (Hansen et al., 2011; Johnson, et al., 2018; Loeb et al.,
255 2012; Trenberth & Fasullo, 2010; von Schuckmann et al., 2016, Meyssignac et al., 2019). The
256 near-global coverage of the Argo network also provides an excellent test bed for the long-term
257 OHC reconstruction extending back well before the Argo period (Cheng et al., 2017). Moreover,
258 these evaluations inform further observing system recommendations for global climate studies, i.e.
259 gaps in the deep ocean layers below 2000m depth, in marginal seas, in shelf areas and in the polar
260 regions (e.g. von Schuckmann et al., 2016), and their implementations are underway, for example
261 for deep Argo (Johnson et al., 2019).

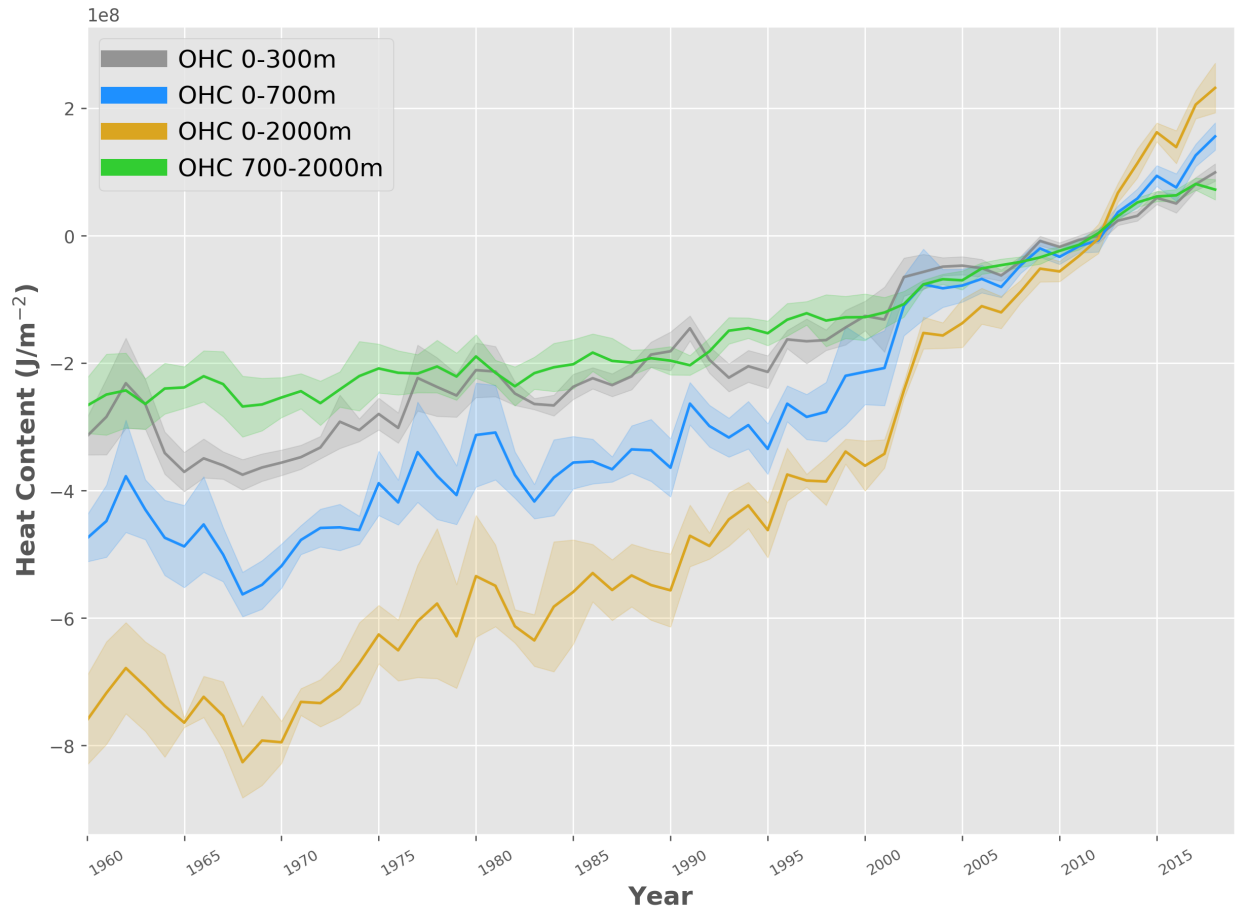
262
263 Different research groups have developed gridded products of subsurface temperature fields for
264 the global ocean using statistical models (Gaillard et al., 2016; Good et al., 2013; Ishii et al., 2017;
265 Levitus et al., 2012) or combined observations with additional statistics from climate models
266 (Cheng et al., 2017). An exhaustive list of the pre-Argo products can be found in for example
267 Abraham et al., 2013; Boyer et al., 2016; WCRP, 2018; Meyssignac et al., 2019. Additionally,
268 specific Argo-based products are listed on the Argo webpage (<http://www.argo.ucsd.edu/>).
269 Although all products rely more or less on the same database, near-global OHC estimates show
270 some discrepancies which result from the different statistical treatments of data gaps, the choice
271 of the climatology and the approach used to account for the MBT and XBT instrumental biases
272 (Boyer et al., 2016; Wang et al., 2018). Argo-based products show smaller differences, likely
273 resulting from different treatments of currently under-sampled regions (e.g. von Schuckmann et
274 al., 2016). Ocean reanalysis systems have been also used to deliver estimates of near-global OHC
275 (Meyssignac et al., 2019; von Schuckmann et al., 2018), and their international assessments show
276 increased discrepancies with decreasing in situ data availability for the assimilation (Palmer et al.,
277 2017; Storto et al., 2018). Climate models have also been used to study global and regional ocean
278 heat changes and the associated mechanisms, with observational datasets providing valuable
279 benchmarks for model evaluation (Cheng et al., 2016; Gleckler et al., 2016).

280
281 International near-global OHC assessments have been performed previously (e.g. Abraham et al.,
282 2013; Boyer et al., 2016; Meyssignac et al., 2019; WCRP, 2018). These assessments are
283 challenging, as most of the gridded temperature fields are research products, and only few are
284 distributed and regularly updated operationally (e.g. <https://marine.copernicus.eu/>). This initiative
285 relies on the availability of data products, their temporal extensions, and direct interactions with
286 the different research groups. A complete view of all international temperature products can be

287 only achieved through a concerted international effort, and over time. In this study, we do not
288 achieve a holistic view of all available products, but present a starting point for future international
289 regular assessments of near-global OHC. For the first time, we propose an international ensemble
290 mean and standard deviation of near-global OHC (Fig. 1) which is then used to build an Earth
291 climate system energy inventory (section 5). The ensemble spread gives an indication of the
292 agreement among products and can be used as a proxy for uncertainty. The basic assumption for
293 the error distribution is Gaussian with a mean of zero, which can be approximated by an ensemble
294 of various products. However, it does not account for systematic errors that may result in biases
295 across the ensemble and does not represent the full uncertainty. The uncertainty can also be
296 estimated in other ways including some purely statistical methods (Levitus et al., 2012) or methods
297 explicitly accounting for the error sources (Lyman & Johnson, 2013), but each method has its
298 caveats, for example the error covariances are mostly unknown, so adopting a straightforward
299 method with a “data democracy” strategy has been chosen here as a starting point.

300
301 However, future evolution of this initiative is needed to include missing and updated in situ-based
302 products, ocean reanalyses, as well as indirect estimates (for example satellite-based). The
303 continuity of this activity will help to further unravel uncertainties due to the community’s
304 collective efforts on detecting/reducing errors, and then provides up-to-date scientific knowledge
305 of ocean heat uptake.

306
307



308
 309
 310
 311
 312
 313
 314
 315
 316

Figure 1: Ensemble mean time series and ensemble standard deviation (2-sigma, shaded) of global ocean heat content (OHC) anomalies relative to the 2005-2017 climatology for the 0-300m (grey), 0-700m (blue), 0-2000m (yellow) and 700-2000m depth layer (green). The ensemble mean is an outcome of an international assessment initiative, and all products used are referenced in the legend of Fig. 2. The trends derived from the time series are given in Table 1. Note that values are given for the ocean surface area between 60°S-60°N, and limited to the 300m bathymetry of each product, respectively.

Period	0-300m (W/m ²)	0-700m (W/m ²)	0-2000m (W/m ²)	700-2000m (W/m ²)
1960-2018	0.3 ± 0.03	0.4 ± 0.1	0.5 ± 0.1	0.2 ± 0.03
1993-2018	0.4 ± 0.04	0.6 ± 0.1	0.9 ± 0.1	0.3 ± 0.03
2005-2018	0.4 ± 0.1	0.6 ± 0.1	1.0 ± 0.2	0.4 ± 0.1
2010-2018	0.5 ± 0.1	0.7 ± 0.1	1.3 ± 0.3	0.5 ± 0.1

317 *Table 1: Linear trends (weighted least square fit, see for example von Schuckmann and Le Traon, 2011) as*
318 *derived from the ensemble mean as presented in Fig. 1 for different time intervals, and different integration*
319 *depth. The uncertainty on the trend estimate is given for the 95% confidence level. Note that values are*
320 *given for the ocean surface area between 60°S-60°N, and limited to the 300m bathymetry of each product,*
321 *respectively. See text and Fig. 1 caption for more details on the OHC estimates.*

322

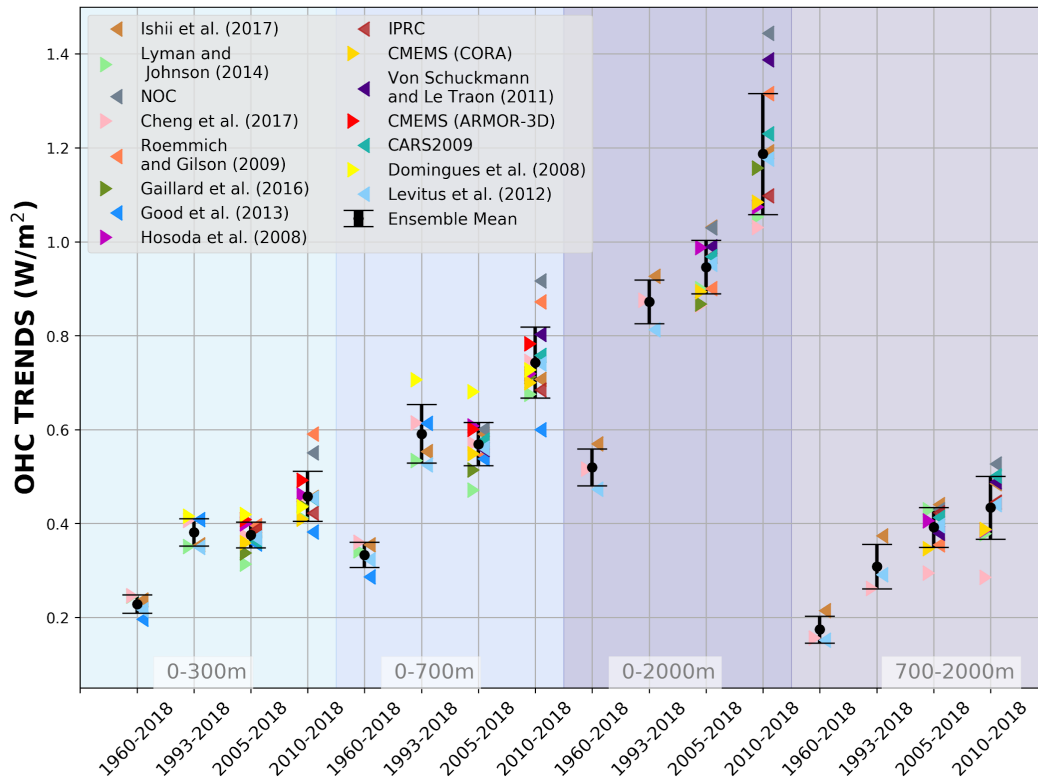
323

324 Products used for this assessment are referenced in the caption of Fig. 2. Estimates of OHC have
325 been provided by the different research groups under homogeneous criteria. All estimates use a
326 coherent ocean volume limited by the 300m isobath of each product, and are limited to 60°S-60°N
327 since most observational products exclude high latitude ocean areas because of the low
328 observational coverage, and only annual averages have been used. 60°S-60°N constitutes ~91%
329 of the global ocean surface area and limiting to 300m isobath neglects the contributions from
330 coastal and shallow waters, so the resultant OHC trends will be underestimated if these ocean
331 regions are warming. For example, neglecting shallow waters can account for 5-10% for 0-2000m
332 OHC trends (von Schuckmann et al., 2014). A first initial test using Cheng et al., (2017) data
333 indicates that OHC 0-2000m trends can be underestimated by ~10% if the ocean warming in the
334 area polewards of 60° latitude is not taken into account (not shown). This is a caveat of the
335 assessment in this review and will be addressed in the future.

336

337 The assessment is based on three distinct periods to account for the evolution of the observing
338 system, i.e. 1960-2018 (i.e. ‘historical’), 1993-2018 (i.e. ‘altimeter era’) and 2005-2018 (i.e.
339 ‘golden Argo-era’). In addition, ocean warming rates over the past decade are specifically
340 discussed according to an apparent acceleration of global surface warming since 2010 (WMO,
341 2020; Blunden and Arndt, 2019). All time series reach the end in 2018 – which was one of the
342 principal limitations for the inclusion of some products. Our final estimates of OHC for the upper
343 2000m over different periods are the ensemble average of all products, with the uncertainty range
344 defined by the standard deviation (2-sigma) of the corresponding estimates used (Fig. 1).

345



346
 347 **Figure 2:** Linear trends of global ocean heat content (OHC) as derived from different temperature products
 348 (colors). References are given in the figure legend, except for IPRC
 349 (<http://apdr.c.soest.hawaii.edu/projects/Argo/>), CMEMS (CORA & ARMOR-3D,
 350 <http://marine.copernicus.eu/science-learning/ocean-monitoring-indicators>), CARS2009
 351 (<http://www.marine.csiro.au/~dunn/cars2009/>) and NOC (National Oceanographic Institution, (D. G.
 352 Desbruyères et al., 2016). The ensemble mean and standard deviation (2-sigma) is given in black,
 353 respectively. The shaded areas show trends from different depth layer integrations, i.e. 0-300m (light
 354 turquoise), 0-700m (light blue), 0-2000m (purple) and 700-2000m (light purple). For each integration
 355 depth layer, trends are evaluated over the three study periods, i.e. historical (1960-2018), altimeter era
 356 (1993-2018) and golden Argo era (2005-2018). In addition, the most recent period 2010-2018 is included.
 357 See text for more details on the international assessment criteria. Note that values are given for the ocean
 358 surface area (see text for more details).

359
 360
 361 The first and principal result of the assessment (Fig. 1) is an overall increase of the trend for the
 362 more recent two study periods e.g., the altimeter era (1993-2018) and golden Argo era (2005-2018)
 363 relative to the historical era (1960-2018), which is in agreement with previous results (e.g.
 364 Abraham et al., 2013). The trend values are all given in Table 1. A major part of heat is stored in
 365 the upper layers of the ocean (0-300m and 0-700m depth). However, heat storage at intermediate
 366 depth (700-2000m) increases at a comparable rate as reported for the 0-300m depth layer (Table

367 1, Fig. 2). There is a general agreement among the 15 international OHC estimates (Fig. 2).
368 However, for some periods and depth layers the standard deviation reaches maximal values up to
369 about 0.3 W/m^2 . All products agree on the fact that ocean warming rates have increased in the past
370 decades, and doubled since the beginning of the altimeter era (1993-2018 compared with 1960-
371 2018) (Fig. 2). Moreover, there is a clear indication that heat sequestration into the deeper ocean
372 layers below 700m depth took place over the past 6 decades linked to an increase of OHC trends
373 over time (Fig. 2). In agreement with observed accelerated Earth surface warming over the past
374 decade (WMO, 2020; Blunden and Arndt, 2019), ocean warming rates for the 0-2000m depth layer
375 also reached record rates of $1.3 (0.9) \pm 0.3 \text{ W/m}^2$ for the ocean (global) area over the period 2010-
376 2018.

377
378 For the deep OHC changes below 2000m, we adapted an updated estimate from (Purkey &
379 Johnson, 2010) (PG10) from 1991 to 2018, which is a constant linear trend estimate (1.15 ± 0.57
380 ZJ/year , $0.07 \pm 0.04 \text{ W/m}^2$). Some recent studies strengthened the results in PG10 (D. G.
381 Desbruyères et al., 2016; Zanna et al., 2019). Desbruyères et al., (2016) examined the decadal
382 change of the deep and abyssal OHC trends below 2000m in 1990s and 2000s, suggesting that
383 there has not been a significant change in the rate of decadal global deep/abyssal warming from
384 the 1990's to the 2000's and the overall deep ocean warming rate is consistent with PG10. Using a
385 Green Function method, Zanna et al. (2019) reported a deep ocean warming rate of $\sim 0.06 \text{ Wm}^{-2}$
386 during the 2000s, consistent with PG10 used in this study. Zanna et al. (2019) shows a fairly weak
387 global trend during the 1990s, inconsistent with observation-based estimates. This mismatch might
388 come from the simplified or misrepresentation of surface-deep connections using ECCO reanalysis
389 data and the use of time-mean Green's functions in Zanna et al. (2019), as well as from the limited
390 spatial resolution of the observational network for relatively short time-spans. Furthermore,
391 combining hydrographic and deep-Argo floats, a recent study (Johnson et al., 2019) reported an
392 accelerated warming in the South Pacific Ocean in recent years, but a global estimate of the OHC
393 rate of change over time is not available yet.

394
395 Before 1990, we assume zero OHC trend below 2000m, following the methodology in IPCC-AR5
396 (Rhein et al., 2013). The zero-trend assumption is made mainly because there are too few
397 observations before 1990 to make an estimate of OHC change below 2000m. But it is a reasonable
398 assumption because OHC 700-2000m warming was fairly weak before 1990 and heat might not
399 have penetrated down to 2000m (Cheng et al., 2017). Zanna et al. (2019) also shows a near zero
400 OHC trend below 2000m from the 1960s to 1980s. The derived time series is used for the Earth
401 energy inventory in section 5. A centralized (around the year 2006) uncertainty approach has been
402 applied for the deep ($> 2000\text{m}$ depth) OHC estimate following the method of Cheng et al., (2017),
403 which allows to extract an uncertainty range over the period 1993-2018 within the given [lower
404 ($1.15 - 0.57 \text{ ZJ/year}$), upper ($1.15 + 0.57 \text{ ZJ/year}$)] range of the deep OHC trend estimate. We then
405 extend the obtained uncertainty estimate back from 1993 to 1960, with 0 OHC anomaly.

406

407

408 **2. Heat available to warm the atmosphere**

409

410 While the amount of heat accumulated in the atmosphere is small compared to the ocean, warming
411 of the Earth's near-surface air and atmosphere aloft is a very prominent effect of climate change,
412 which directly affects society. Atmospheric observations clearly reveal a warming of the
413 troposphere over the last decades (Santer et al., 2017; Steiner et al., 2020) and changes in the
414 seasonal cycle (Santer et al., 2018). Changes in atmospheric circulation (Cohen et al., 2014; Fu et
415 al., 2019) together with thermodynamic changes (Fischer & Knutti, 2016; Trenberth et al., 2015)
416 will lead to more extreme weather events and increase high impact risks for society (Coumou et
417 al., 2018; Zscheischler et al., 2018). Therefore, a rigorous assessment of the atmospheric heat
418 content in context with all Earth's climate subsystems is important for a full view on the changing
419 climate system.

420

421 The atmosphere transports vast amounts of energy laterally and strong vertical heat fluxes occur
422 at the atmosphere's lower boundary. The pronounced energy and mass exchanges within the
423 atmosphere and with all other climate components is a fundamental element of Earth's climate
424 (Peixoto & Oort, 1992). In contrast, long-term heat accumulation in the atmosphere is limited by
425 its small heat capacity as the gaseous component of the Earth system (von Schuckmann et al.,
426 2016).

427 Recent work revealed inconsistencies in earlier formulations of the atmospheric energy budget
428 (Mayer et al., 2017; Trenberth & Fasullo, 2018), and hence a short discussion of the updated
429 formulation is provided here. In a globally averaged and vertically integrated sense, heat
430 accumulation in the atmosphere arises from a small imbalance between net energy fluxes at the
431 top of the atmosphere (TOA) and the surface (denoted s). The heat budget of the vertically
432 integrated and globally averaged atmosphere (indicated by the global averaging operator $\langle \cdot \rangle$) reads
433 as follows (Mayer et al., 2017):

$$434 \quad \left\langle \frac{\partial AE}{\partial t} \right\rangle = \langle N_{TOA} \rangle - \langle F_s \rangle - \langle F_{snow} \rangle - \langle F_{PE} \rangle, \quad (2)$$

435 where, in mean-sea-level altitude (z) coordinates used here for integrating over observational
436 data, the vertically integrated atmospheric energy content AE per unit surface area [Jm^{-2}] reads

$$437 \quad AE = \int_{z_s}^{z_{TOA}} \rho (c_v T + g(z - z_s) + L_e q + \frac{1}{2} V^2) dz. \quad (3)$$

438 In Equation 2, AE represents the total atmospheric energy content, N_{TOA} the net radiation at top-
439 of-the-atmosphere, F_s net surface energy flux defined as the sum of net surface radiation and latent
440 and sensible heat flux, and F_{snow} the latent heat flux associated with snowfall (computed as the
441 product of latent heat of fusion and snowfall rate). Here, we take constant latent heat of
442 vaporization (at 0°C) in the latent heat flux term that is contained in F_s but variations in latent heat
443 flux arising from the deviation of evaporated water from 0°C are contained in F_{PE} , which
444 additionally accounts for sensible heat of precipitation (referenced to 0°C). That is, F_{PE} expresses

445 a modification of F_s arising from global evaporation and precipitation occurring at temperatures
446 different from 0°C .

447 Snowfall is the fraction of precipitation that returns originally evaporated water to the surface in a
448 frozen state. In that sense, F_{snow} represents a heat transfer from the surface to the atmosphere: it
449 warms the atmosphere through additional latent heat release (associated with freezing of vapor)
450 and snowfall consequently arrives at the surface in an energetic state lowered by this latent heat.
451 This energetic effect is most obvious over the open ocean, where falling snow requires the same
452 amount of latent heat to be melted again and thus cools the ocean. Over high latitudes, F_{snow} can
453 attain values up to 5 Wm^{-2} , but its global average value is smaller than 1 Wm^{-2} (Mayer et al., 2017).
454 Although its global mean energetic effect is relatively small, it is systematic and should be included
455 for accurate diagnostics. Moreover, snowfall is an important contributor to the heat and mass
456 budget of ice sheets and sea ice (see section 4).

457 F_{PE} represents the net heat flux arising from the different temperatures of rain and evaporated
458 water. This flux can be sizable regionally, but it is small in a global average sense (warming of the
459 atmosphere $\sim 0.3 \text{ Wm}^{-2}$ according to Mayer et al., 2017).

460 Equation 3 provides a decomposition of the atmospheric energy content AE into sensible heat
461 energy (sum of the first two terms, internal heat energy and gravity potential energy), latent heat
462 energy (third term) and kinetic energy (fourth term), where ρ is the air density, c_v the specific heat
463 for moist air at constant volume, T the air temperature, g the acceleration of gravity, L_e the
464 temperature-dependent effective latent heat of condensation (and vaporization) L_v or sublimation
465 L_s (the latter relevant below 0°C), q the specific humidity of the moist air, and V the wind speed.
466 We neglect atmospheric liquid water droplets and ice particles as separate species, as their amounts
467 and especially their trends are small.

468 In the AE derivation from observational datasets based on Equation 3, we accounted for the
469 intrinsic temperature dependence of the latent heat of water vapor by assigning L_e to L_v if ambient
470 temperatures are above 0°C and to L_s (adding in the latent heat of fusion L_f) if they are below -10
471 $^\circ\text{C}$, respectively, with a gradual (half-sine weighted) transition over the temperature range
472 between. The reanalysis evaluations similarly approximated L_e by using values of L_v , L_s , and L_f ,
473 though in slightly differing forms. The resulting differences in AE anomalies from any of these
474 choices are negligibly small, however, since the latent heat contribution at low temperatures is
475 itself very small.

476 As another small difference, the AE estimations from observations neglected the kinetic energy
477 term in Equation 3 (fourth term), while the reanalysis evaluations accounted for it. This as well
478 leads to negligible AE anomaly differences, however, since the kinetic energy content and trends
479 at global scale are more than three orders of magnitude smaller than for the sensible heat (Peixoto
480 and Oort, 1992). Aligning with the terminology of ocean heat content (OHC) and given the
481 dominance of the heat-related terms in Equation 3, we hence refer to the energy content AE as
482 atmospheric heat content (AHC) hereafter.

483 Turning to the actual datasets used, atmospheric energy accumulation can be quantified using
484 various data types, as summarized in the following. Atmospheric reanalyses combine

485 observational information from various sources (radiosondes, satellites, weather stations, etc.) and
486 a dynamical model in a statistically optimal way. This data type has reached a high level of
487 maturity, thanks to continuous development work since the early 1990s (Hersbach et al., 2018).
488 Especially reanalysed atmospheric state quantities like temperature, winds, and moisture are
489 considered to be of high quality and suitable for climate studies, although temporal discontinuities
490 introduced from the ever-changing observation system remain a matter of concern (Berrisford et
491 al., 2011; Chiodo & Haimberger, 2010).

492 Here we use the current generation of atmospheric reanalyses as represented by ECMWF's fifth-
493 generation reanalysis ERA5 (Hersbach et al., 2018, 2020), NASA's Modern-Era Retrospective
494 analysis for Research and Applications version 2 (MERRA2) (Gelaro et al., 2017), and JMA's 55-
495 year-long reanalysis JRA55 (Kobayashi et al., 2015). All these are available over 1980 to 2018
496 (ERA5 also in 1979) while JRA55 is the only one covering the full early timeframe 1960 to 1979.
497 We additionally used a different version of JRA55 that assimilates only conventional observations
498 also over the satellite era from 1979 onwards, which away from the surface only leaves radiosondes
499 as data source and which is available to 2012 (JRA55C). The advantage of this product is that it
500 avoids potential spurious jumps associated with satellite changes. Moreover, JRA55C is fully
501 independent of satellite-derived Global Positioning System (GPS) radio occultation (RO) data that
502 are also separately used and described below together with the observational techniques.

503 In addition to these four reanalyses, the datasets from three different observation techniques have
504 been used for complementary observational estimates of the atmospheric heat content (AHC). We
505 use the Wegener Center (WEGC) multi-satellite RO data record, WEGC OPSv5.6 (Angerer et al.,
506 2017) as well as its radiosonde (RS) data record derived from the high-quality Vaisala sondes
507 RS80/RS92/VS41, WEGC Vaisala (Ladstädter et al., 2015). WEGC OPSv5.6 and WEGC Vaisala
508 provide thermodynamic upper air profiles of air temperature, specific humidity, and density from
509 which we locally estimate the vertical AHC based on the first three integral terms of Equation 3
510 (Kirchengast et al., 2019). In atmospheric domains not fully covered by the data (e.g., in the lower
511 part of the boundary layer for RO or over the polar latitudes for RS) the profiles are vertically
512 completed by collocated ERA5 information. The local vertical AHC results are then averaged into
513 regional monthly means, which are finally geographically aggregated to global AHC. Applying
514 this estimation approach in the same way to reanalysis profiles sub-sampled at the observation
515 locations accurately leads to the same AHC anomaly time series records as the direct estimation
516 from the full gridded fields.

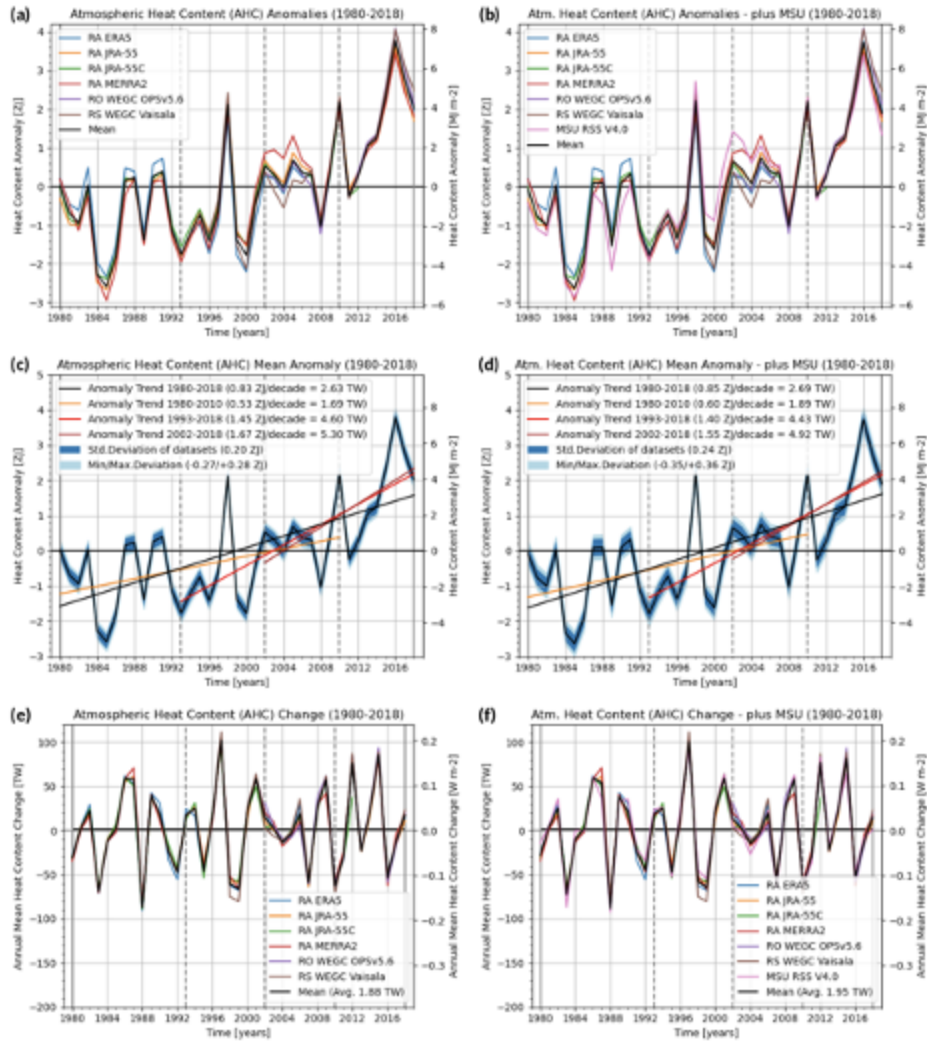
517 The third observation-based AHC dataset derives from a rather approximate estimation approach
518 using the microwave sounding unit (MSU) data records (Mears & Wentz, 2017). Because the very
519 coarse vertical resolution of the brightness temperature measurements from MSU does not enable
520 integration according to Equation 3, this dataset is derived by replicating the method used in IPCC
521 AR5 WGI Assessment Report 2013 (Rhein, M., et al., 2013; Chap. 3, Box 3.1 therein). We used
522 the most recent MSU Remote Sensing System (RSS) V4.0 temperature dataset (Mears and Wentz,
523 2017), however, instead of MSU RSS V3.3 that was used in the IPCC AR5 (Mears & Wentz,
524 2009a, 2009b) (updated to version 3.3). In order to derive global time series of AHC anomalies,
525 the approach simply combines weighted MSU lower tropospheric temperature and lower
526 stratospheric temperature changes (TLT and TLS channels) converted to sensible heat content

527 changes via global atmospheric mass, and an assumed fractional increase of latent heat content
528 according to water vapor content increase driven by temperature at a near-Clausius-Clapeyron rate
529 (7.5 %/°C).

530 Figure 3 shows the resulting global AHC change inventory over 1980 to 2018 in terms of AHC
531 anomalies of all data types (top), mean anomalies and time-average uncertainty estimates including
532 long-term AHC trend estimates (middle), and annual-mean AHC tendency estimates (bottom). The
533 mean anomaly time series (middle left), preceded by the small JRA55 anomalies over 1960-1979
534 is used as part of the overall heat inventory in Section 5 below. Results including MSU in addition
535 are separately shown (right column), since this dataset derives from a fairly approximate
536 estimation as summarized above and hence is given lower confidence than the others deriving from
537 rigorous AHC integration & aggregation. Since it was the only dataset for AHC change estimation
538 in the IPCC AR5 report, bringing it into context is considered relevant, however.

539 The results clearly show that the AHC trends have intensified from the earlier decades represented
540 by the 1980-2010 trends of near 1.8 TW (consistent with the trend interval used in the IPCC AR5
541 report). We find the trends about 2.5 times higher over 1993-2018 (about 4.5 TW) and about three
542 times higher in the most recent two decades over 2002-2018 (near 5.3 TW), a period that is already
543 fully covered also by the RO and RS records (which estimate around 6 TW). Checking the
544 sensitivity of these long-term trend estimates to ENSO interannual variations, by comparing trend
545 fits to ENSO-corrected AHC anomalies (with ENSO regressed out via the Nino 3.4 Index),
546 confirms that the estimates are robust.

547 The year-to-year annual-mean tendencies in AHC, reaching amplitudes as high as 50 to 100 TW
548 (or 0.1 to 0.2 Wm⁻², if normalized to the global surface area), indicate the strong coupling of the
549 atmosphere with the uppermost ocean. This is mainly caused by the ENSO interannual variations
550 that lead to net energy changes in the climate system including the atmosphere (Loeb et al., 2012;
551 Mayer et al., 2013) and substantial reshuffling of heat energy between the atmosphere and the
552 upper ocean (Lijing Cheng, Trenberth, et al., 2019; Johnson & Birnbaum, 2017; Mayer et al., 2014,
553 2016).



554
 555 **Figure 3:** Annual-mean global AHC anomalies over 1980 to 2018 of four different reanalyses and two (left)
 556 or three (right, plus MSU) different observational datasets shown together with their mean (top), the mean
 557 AHC anomaly shown together with four representative AHC trends and ensemble spread measures of its
 558 underlying datasets (middle), and the annual-mean AHC change (annual tendency) shown for each year
 559 over 1980 to 2018 for all datasets and their mean (bottom). The in-panel legends identify the individual
 560 datasets shown (top and bottom) and the chosen trend periods together with the associated trend values
 561 and spread measures (middle), the latter including the time-average standard deviation and
 562 minimum/maximum deviations of the individual datasets from the mean.

563
 564
 565 **3. Heat available to warm land**

566
 567 Although the land component of the Earth's energy budget accounts for a small proportion of heat
 568 in comparison with the ocean, several land-based processes sensitive to the magnitude of the
 569 available land heat play a crucial role in the future evolution of climate. Among others, the stability

570 and extent of the continental areas occupied by permafrost soils depend on the land component.
571 Alterations of the thermal conditions at these locations have the potential to release long-term
572 stored CO₂ and CH₄, and may also destabilize the recalcitrant soil carbon (Bailey et al., 2019;
573 Hicks Pries et al., 2017). Both of these processes are potential "tipping points" (Lenton et al., 2019;
574 Lenton, 2011; Lenton et al., 2008) leading to possible positive feedback on the climate system
575 (Leifeld et al., 2019; MacDougall et al., 2012). Increased land energy is related to decreases in soil
576 moisture that may enhance the occurrence of extreme temperature events (Jeong et al., 2016; S.
577 Seneviratne et al., 2006, 2014; S. I. Seneviratne et al., 2010; Xu et al., 2019). Such extreme events
578 carry negative health effects for the most vulnerable sectors of human and animal populations and
579 ecosystems (Matthews et al., 2017; McPherson et al., 2017; Sherwood & Huber, 2010; Watts et
580 al., 2019). Given the importance of properly determining the fraction of EEI flowing into the land
581 component, recent works have examined the CMIP5 simulations and revealed that Earth System
582 Models (ESMs) have shortcomings in modelling the land heat content of the last half of the 20th
583 century (Francisco José Cuesta-Valero et al., 2016). Numerical experiments have pointed to an
584 insufficient depth of the Land Surface Models (LSMs) (MacDougall et al., 2008, 2010; C. W.
585 Stevens, 2007) and to a zero heat-flow bottom boundary condition (BBC) as the origin of the
586 limitations in these simulations. An LSM of insufficient depth limits the amount of energy that can
587 be stored in the subsurface. The zero heat-flow BBC neglects the small but persistent long-term
588 contribution from the flow of heat from the interior of the Earth, that shifts the thermal regime of
589 the subsurface towards or away from the freezing point of water, such that the latent heat
590 component is misrepresented in the northern latitudes (Hermoso de Mendoza et al., 2018).
591 Although the heat from the interior of the Earth is constant at time scales of a few millennia, it
592 may conflict with the setting of the LSM initial conditions in ESM simulations. Modelling
593 experiments have also allowed to estimate the heat content in land water reservoirs (Vanderkelen
594 et al., 2020), accounting for 0.3 ± 0.3 ZJ from 1900 to 2020. Nevertheless, this estimate has not
595 been included here because it is derived from model simulations and its magnitude is small in
596 relation to the rest of components of the Earth's heat inventory.
597

598 **Borehole Climatology**

599 The main premise of borehole climatology is that the subsurface thermal regime is determined by
600 the balance of the heat flowing from the interior of the Earth (the bottom boundary condition) and
601 the heat flowing through the interface between the lower atmosphere and the ground (the upper
602 boundary condition). If the thermal properties of the subsurface are known, or if they can be
603 assumed constant over short-depth intervals, then the thermal regime of the subsurface can be
604 determined by the physics of heat diffusion. The simplest analogy is the temperature distribution
605 along a (infinitely wide) cylinder with known thermal properties and constant temperature at both
606 ends. If upper and lower boundary conditions remain constant (i.e. internal heat flow is constant,
607 and there are no persistent variations on the ground surface energy balance), then the thermal

608 regime of the subsurface is well known and it is in a (quasi) steady state. However, any change to
609 the ground surface energy balance would create a transient, and such a change in the upper
610 boundary condition would propagate into the ground leading to changes in the thermal regime of
611 the subsurface (Beltrami, 2002a). These changes in the ground surface energy balance propagate
612 into the subsurface and are recorded as departures from the quasi-steady thermal state of the
613 subsurface. Borehole climatology uses these subsurface temperature anomalies to reconstruct the
614 ground surface temperature changes that may have been responsible for creating the subsurface
615 temperature anomalies we observe. That is, it is an attempt to reconstruct the temporal evolution
616 of the upper boundary condition. Ground Surface Temperature Histories (GSTHs) and Ground
617 Heat Flux Histories (GHFHs) have been reconstructed from borehole temperature profile (BTP)
618 measurements at regional and larger scales for decadal and millennial time-scales (Barkaoui et al.,
619 2013; Beck, 1977; Beltrami, 2001; Beltrami et al., 2006; Beltrami & Bourlon, 2004; Cermak,
620 1971; Christian Chouinard & Mareschal, 2009; Davis et al., 2010; Demezhko & Gornostaeva,
621 2015; Harris & Chapman, 2001; Hartmann & Rath, 2005; Hopcroft et al., 2007; Huang et al., 2000;
622 Jaume-Santero et al., 2016; Lachenbruch & Marshall, 1986; Lane, 1923; Pickler et al., 2018; Roy
623 et al., 2002; Vasseur et al., 1983). These reconstructions have provided independent records for
624 the evaluation of the evolution of the climate system well before the existence of meteorological
625 records. Because subsurface temperatures are a direct measure, which unlike proxy reconstructions
626 of past climate do not need to be calibrated with the meteorological records, they provide an
627 independent way of assessing changes in climate. Such records, are useful tools for evaluating
628 climate simulations prior to the observational period (Beltrami et al., 2017; Cuesta-Valero et al.,
629 2019; Cuesta-Valero et al., 2016; García-García et al., 2016; González-Rouco et al., 2006; Jaume-
630 Santero et al., 2016; MacDougall et al., 2010; Stevens et al., 2008), as well as for assessing proxy
631 data reconstructions (Beltrami et al., 2017; Jaume-Santero et al., 2016).

632
633 Borehole reconstructions have, however, certain limitations. Due to the nature of heat diffusion,
634 temperature changes propagated through the subsurface suffer both a phase shift and an amplitude
635 attenuation (Smerdon & Stieglitz, 2006). Although subsurface temperatures continuously record
636 all changes in the ground surface energy balance, heat diffusion filters out the high frequency
637 variations of the surface signal with depth, thus the annual cycle is detectable up to approximately
638 16 m of depth, while millennial changes are recorded approximately to a depth of 500 m.
639 Therefore, reconstructions from borehole temperature profiles represent changes at decadal to
640 millennial time scales. Additionally, borehole data are sparse, since the logs were usually recorded
641 from holes of opportunity at mining exploration sites. As a result, the majority of profiles were
642 measured in the Northern Hemisphere, although recent efforts have been taken to increase the
643 sampling rate in South America (Pickler et al., 2018) and Australia (Suman et al., 2017). Despite
644 this uneven sampling, the spatial distribution of borehole profiles has been able to represent the
645 evolution of land surface conditions at global scales (Beltrami & Bourlon, 2004; Cuesta-Valero et
646 al., 2020; González-Rouco et al., 2006, 2009; Pollack & Smerdon, 2004). Another factor that
647 reduces the number of borehole profiles suitable for climate analyses is the presence of non-

648 climatic signals in the measured profiles, mainly caused by groundwater flow and changes in the
 649 lithology of the subsurface. Therefore, all profiles are screened before the analysis in order to
 650 remove questionable logs. Despite all these limitations, the borehole methodology has been shown
 651 to be reliable based on observational analyses (Bense & Kooi, 2004; C Chouinard & Mareschal,
 652 2007; Pollack & Smerdon, 2004; Verdoya et al., 2007) and pseudo-proxy experiments
 653 (García Molinos et al., 2016; González-Rouco et al., 2006, 2009).

654

655 **Land Heat Content Estimates**

656

657 Global continental energy content has been previously estimated from geothermal data retrieved
 658 from a set of quality-controlled borehole temperature profiles. Ground heat content was estimated
 659 from heat flux histories derived from BTP data (Beltrami, 2002b; Beltrami et al., 2002, 2006).
 660 Such results have formed part of the estimate used in AR3, AR4 and AR5 IPCC reports (see Box
 661 3.1, Chapter 3 (Rhein et al., 2013). A continental heat content estimate was inferred from
 662 meteorological observations of surface air temperature since the beginning of the 20th century
 663 (Huang, 2006). Nevertheless, all global estimates were performed nearly two decades ago. Since,
 664 those days, advances in borehole methodological techniques (Beltrami et al., 2015; Cuesta-Valero
 665 et al., 2016; Jaume-Santero et al., 2016), the availability of additional BTP measurements, and the
 666 possibility of assessing the continental heat fluxes in the context of the FluxNet measurements
 667 (Gentine et al., 2020) requires a comprehensive summary of all global ground heat fluxes and
 668 continental heat content estimates.

669

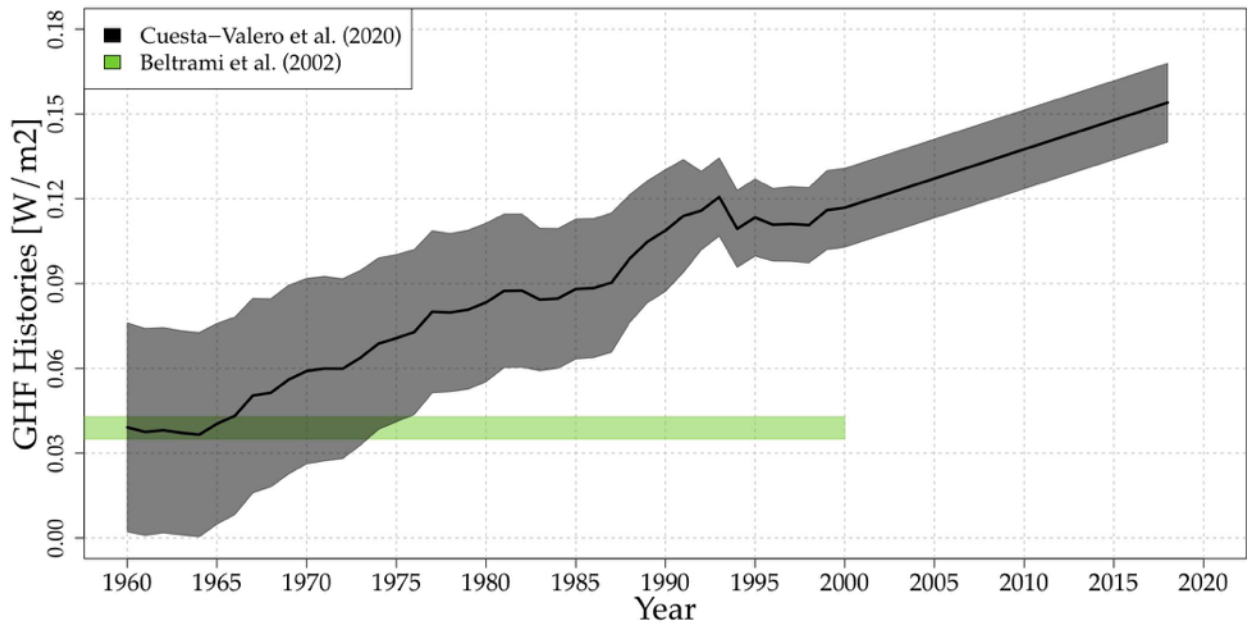
Reference	Time period	Heat Flux (mWm ⁻²)	Heat Content (ZJ)	Source of Data
(Beltrami, 2002b)	1950-2000	33	7.1	Geothermal
Beltrami et al. (2002)	1950-2000	39.1 (3.5)	9.1 (0.8)	Geothermal
Beltrami et al. (2002)	1900-2000	34.1 (3.4)	15.9 (1.6)	Geothermal
(Beltrami, 2002b)	1765-2000	20.0 (2.0)	25.7 (2.6)	Geothermal
Huang (2006)	1950-2000	-	6.7	Meteorological
Gentine et al (2020)	2004-2015	240 (120)	-	FluxNet, Geothermal, LSM
Cuesta-Valero et al (2020)	1950-2000	70 (20)	16 (3)	Geothermal
Cuesta-Valero et al (2020)	1993-2018	129 (28)	14 (3)	Geothermal
Cuesta-Valero et al., (2020)	2004-2015	136 (28)	6 (1)	Geothermal

670 *Table 2. Ground surface heat flux and global continental heat content. Uncertainties in parenthesis.*

671

672

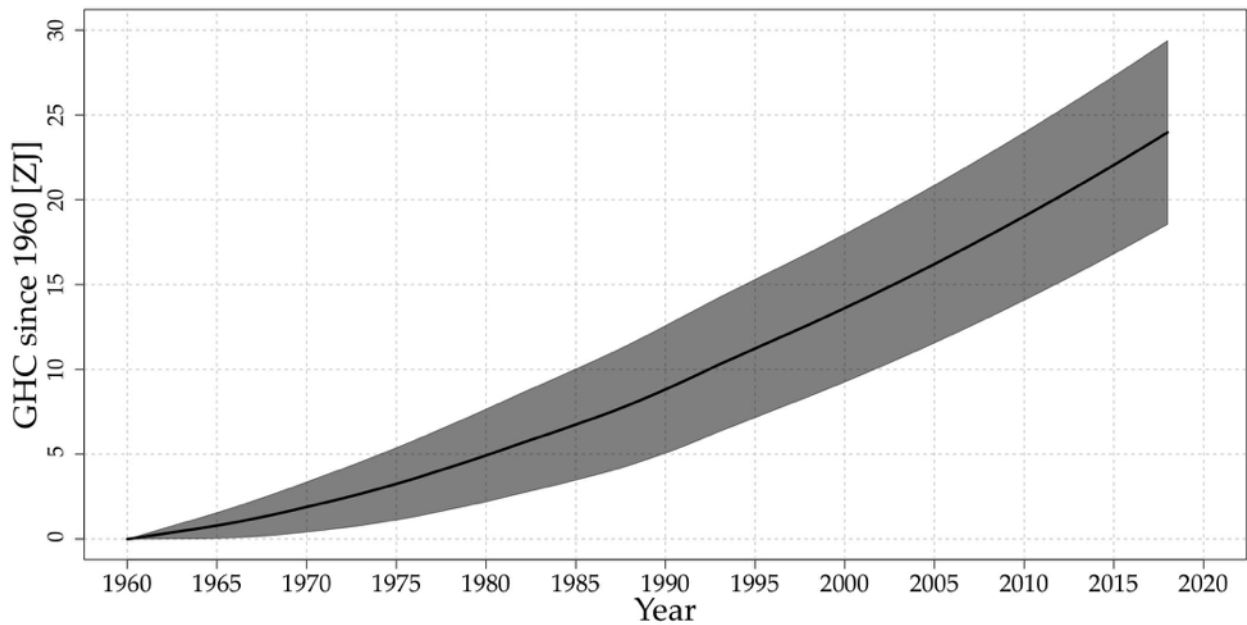
673



674

675 **Figure 4:** Global mean ground heat flux history (black line) and 95% confidence interval (gray shadow)
676 from BTP measurements from Cuesta-Valero et al. (2020). Results for 1950-2000 from Beltrami et al.
677 (2002) (green bar) are provided for comparison purposes.

678



679

680 **Figure 5:** Global cumulative heat storage within continental landmasses since 1960 CE (black line) and
681 95% confidence interval (gray shadow) estimated from GHF results displayed in Fig.4. Data obtained from
682 Cuesta-Valero et al. (2020).

683 The first estimates of continental heat content used borehole temperature versus depth profile data.
684 However, the dataset in those analyses included borehole temperature profiles of a wide range of
685 depths, as well as different data acquisition dates. That is, each borehole profile contained the
686 record of the accumulation of heat in the subsurface for different time intervals. In addition, the
687 borehole data were analyzed for a single ground surface temperature model using a single constant
688 value for each of the subsurface thermal properties.

689 Although the thermal signals are attenuated with depth, which may partially compensate for data
690 shortcomings, uncertainties were introduced in previous analyses that may have affected the
691 estimates of subsurface heat change. A continental heat content change estimate was carried out
692 using a gridded meteorological product of surface air temperature by (Huang, 2006). Such work
693 yielded similar values as the estimates from geothermal data (see Table 2). This estimate, however,
694 assumed that surface air and ground temperatures are perfectly coupled everywhere, and used a
695 single value for the thermal conductivity of the ground. Studies have shown that the coupling of
696 the surface air and ground temperatures is mediated by several processes that may influence the
697 ground surface energy balance, and therefore, the air-ground temperature coupling (García-García
698 et al., 2019; Melo-Aguilar et al., 2018; Stieglitz & Smerdon, 2007). In a novel attempt to reconcile
699 continental heat content from soil heat-plate data from the FluxNet network with estimates from
700 geothermal data and a deep bottom-boundary land surface model simulation, (Gentine et al., 2020)
701 obtained a much larger magnitude from the global land heat flux than all previous estimates.
702 Cuesta-Valero et al. (2020) has recently updated the estimate of the global continental heat content
703 using a larger borehole temperature database (1079 logs) that includes more recent measurements
704 and a stricter data quality control. The updated estimate of continental heat content change also
705 takes into account the differences in borehole logging time and restricts the data to the same depth
706 range for each borehole temperature profile. Such depth range restriction ensures that the
707 subsurface accumulation of heat at all BTP sites is synchronous. In addition to the standard method
708 for reconstructing heat fluxes with a single constant value for each subsurface thermal property,
709 Cuesta-Valero et al. (2020) also developed a new approach that considers a range of possible
710 subsurface thermal properties, several models, each at a range of resolutions yielding a more
711 realistic range of uncertainties for the fraction of the EEI flowing into the land subsurface.

712 Global land heat content estimates from FluxNet data, geothermal data and model simulations
713 point to a marked increase in the amount of energy flowing into the ground in the last few decades
714 (Fig. 4, 5 and Table 2). These results are consistent with the observations of ocean, cryosphere and
715 atmospheric heat storage increases during the same time period and with EEI at the top of the
716 atmosphere.

717

718 **4. Heat utilized to melt ice**

719

720 The energy uptake by the cryosphere is given by the sum of the energy uptake within each one of
721 its components: sea-ice, the Greenland and Antarctic ice sheets, glaciers other than those that are
722 part of the ice sheets ('glaciers', hereafter), snow and permafrost. The basis for the heat uptake by

723 the cryosphere presented here is provided by a recent estimate for the period 1979 to 2017 (F.
724 Straneo et al., 2020). This study concludes that heat uptake over this period is dominated by the
725 mass loss from Arctic sea-ice, glaciers and the Greenland and Antarctic ice sheets. The
726 contributions from thawing permafrost and shrinking snow cover are either negligible, compared
727 to these other components, or highly uncertain. (Note that warming of the land in regions where
728 permafrost is present is accounted for in the land-warming, however, the energy to thaw the
729 permafrost is not). Antarctic sea-ice shows no explicit trend over the period described here
730 (Parkinson, 2019). Here, we extend the estimate of Straneo et al. 2020 backwards in time to 1960
731 and summarize the method, the data and model outputs used. The reader is referred to Straneo et
732 al. (2020) for further details.

733
734 Within each component of the cryosphere, energy uptake is dominated by that associated with
735 melting; including both the latent heat uptake and the warming of the ice to its freezing point. As
736 a result, the energy uptake by each component is directly proportional to its mass loss (Straneo et
737 al., 2020). For consistency with previous estimates (Ciais et al., 2013), we use a constant latent
738 heat of fusion of 3.34×10^5 J/kg, a specific heat capacity of 2.01×10^3 J/kg C and an ice density of
739 920 kg/m^3 .

740
741 For Antarctica, we separate contributions from grounded ice loss and floating ice loss building on
742 recent separate estimates for each. Grounded ice loss from 1992 to 2017 is based on a recent study
743 that reconciles mass balance estimates from gravimetry, altimetry and input-output methods from
744 1992 to 2017 (Shepherd, Ivins, et al., 2018). For the 1972-1991 period, we used estimates from
745 (Rignot et al., 2019), which combined modeled surface mass balance with ice discharge estimates
746 from the input/output method. Floating ice loss between 1994 and 2017 is based on thinning rates
747 and iceberg calving fluxes estimated using new satellite altimetry reconstructions (Adusumilli et
748 al., 2019). For the 1960–1994 period, we also considered mass loss from declines in Antarctic
749 Peninsula ice shelf extent (Cook & Vaughan, 2010) using the methodology described in Straneo
750 et al. (2020).

751
752 To estimate grounded ice mass loss in Greenland, we use the Ice Sheet Mass Balance
753 Intercomparison Exercise for the time period 1992-2017 (Shepherd et al., 2020) and the difference
754 between surface mass balance and ice discharge for the period 1979-1991 (Mankoff et al., 2019;
755 Mougnot et al., 2019; Noël et al., 2018). Due to a lack of observations, from 1960-1978 we
756 assume no mass loss. For floating ice mass change, we collated reports of ice shelf thinning and/or
757 collapse together with observed tidewater glacier retreat (Straneo et al., 2020). Based on firm
758 modeling we assessed that warming of Greenland's firm has not yet contributed significantly to its
759 energy uptake (Ligtenberg et al., 2018; F. Straneo et al., 2020).

760
761 For glaciers we combine estimates for glaciers from the Randolph Glacier Inventory outside of
762 Greenland and Antarctica, based on direct and geodetic measurements (Zemp et al., 2019), with

763 estimates based on a glacier model forced with an ensemble of reanalysis data (Marzeion et al.,
764 2015) and GRACE based estimates (Bamber et al., 2018). An additional contribution from
765 uncharted glaciers or glaciers that have already disappeared is obtained from (Parkes & Marzeion,
766 2018). Greenland and Antarctic peripheral glaciers are derived from Zemp et al., (2019) and
767 Marzeion et al. (2015).

768
769 Finally, while estimates of Arctic sea-ice extent exist over the satellite record, sea-ice thickness
770 distribution measurements are scarce making it challenging to estimate volume changes. Instead
771 we use the Pan-Arctic Ice Ocean Modeling and Assimilation System (PIOMAS) (Schweiger et al.,
772 2011; Zhang & Rothrock, 2003) which assimilates ice concentration and sea surface temperature
773 data and is validated with most available thickness data (from submarines, oceanographic
774 moorings, and remote sensing; and against multi-decadal records constructed from satellite, e.g.
775 (Labe et al., 2018; Laxon et al., 2013; X. Wang et al., 2016). A longer reconstruction using a
776 slightly different model version, PIOMAS-20C (Schweiger et al., 2019), is used to cover the 1960
777 to 1978 period that is not covered by PIOMAS.

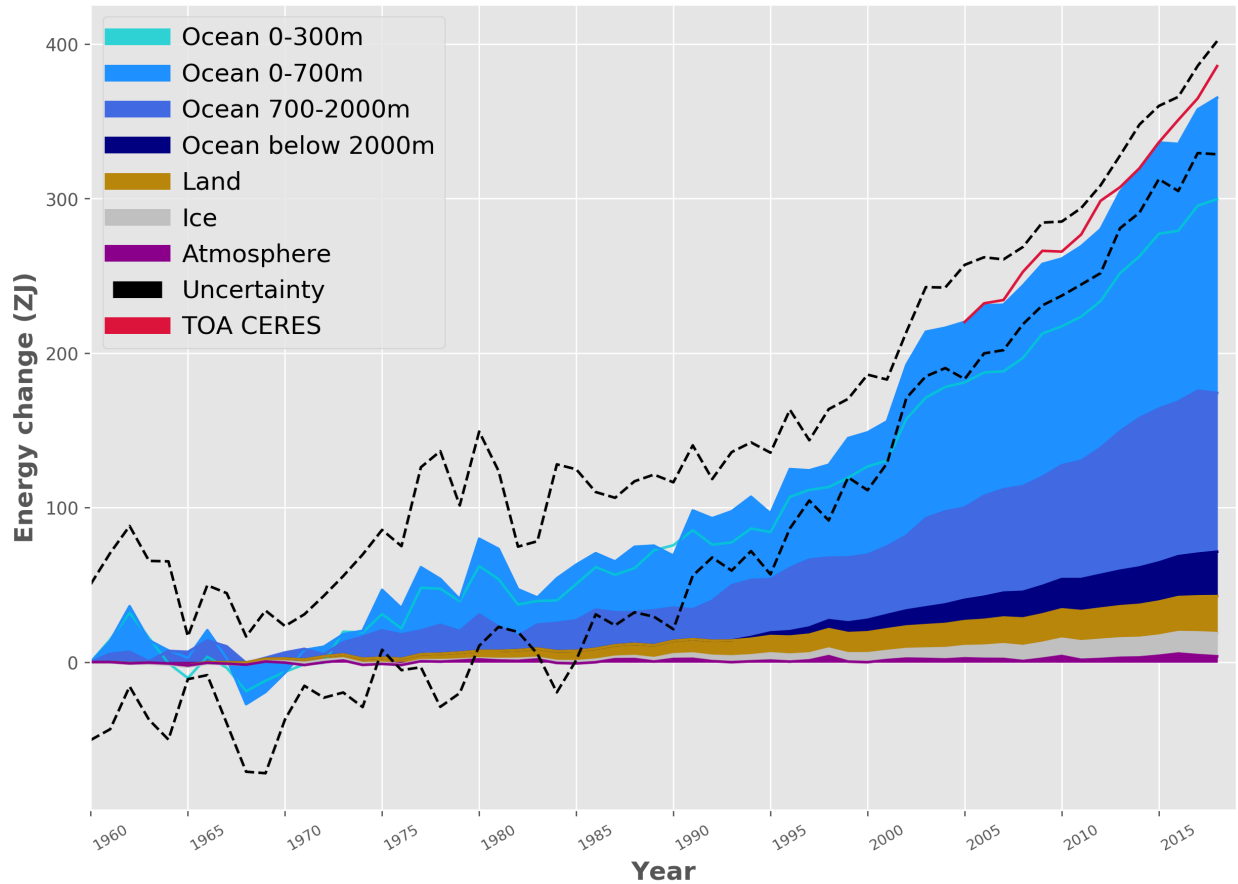
778
779 These reconstructions reveal that all four components contributed similar amounts (between 2-5
780 ZJ) over the 1960-2017 period amounting to a total energy uptake by the cryosphere of 14.7 +/-
781 1.9 ZJ. Compared to earlier estimates, and in particular the 8.83 ZJ estimate from (Ciais et al.,
782 2013), this larger estimate is a result both of the longer period of time considered and, also, the
783 improved estimates of ice loss across all components, especially the ice shelves in Antarctica.
784 Approximately half of the Cryosphere's energy uptake is associated with the melting of grounded
785 ice, while the remaining half is associated with the melting of floating ice (ice shelves in Antarctica
786 and Greenland, Arctic sea-ice).

787
788

789 **5. The Earth heat inventory: Where does the energy go?**

790
791 The Earth has been in radiative imbalance, with less energy exiting the top of the atmosphere than
792 entering, since at least about 1970 and the Earth has gained substantial energy over the past 4
793 decades (Hansen, 2005; Rhein et al., 2013). Due to the characteristics of the Earth system
794 components, the ocean with its large mass and high heat capacity dominates the Earth heat
795 inventory (Cheng et al., 2016, 2017; Rhein et al., 2013; von Schuckmann et al., 2016). The rest
796 goes into grounded and floating ice melt, and warming the land and atmosphere.

797
798



800
 801 **Figure 6:** Earth heat inventory (energy accumulation) in ZJ ($1 \text{ ZJ} = 10^{21} \text{ J}$) for the components of the
 802 Earth's climate system relative to 1960 and from 1960 to 2018 (assuming constant cryosphere increase for
 803 the year 2018). See section 1-4 for data sources. The upper ocean (0-300m, light blue line, and 0-700m,
 804 light blue shading) account for the largest amount of heat gain, together with the intermediate ocean (700-
 805 2000m, blue shading), and the deep ocean below 2000m depth (dark blue shading). Although much lower,
 806 the second largest contributor is the storage of heat on land (orange shading), followed by the gain of heat
 807 to melt grounded and floating ice in the cryosphere (gray shading). Due to its low heat capacity, the
 808 atmosphere (magenta shading) makes a smaller contribution. Uncertainty in the ocean estimate also
 809 dominates the total uncertainty (dot-dashed lines derived from the standard deviations (2-sigma) for the
 810 ocean, cryosphere and land. Atmospheric uncertainty is comparably small). Deep ocean ($> 2000\text{m}$) are
 811 assumed zero before 1990 (see section 1 for more details). The dataset for the Earth heat inventory is
 812 published at DKRZ (<https://www.dkrz.de/>) under the doi:
 813 https://doi.org/10.26050/WDC/GCOS_EHI_EXP_v2. The net flux at TOA from the NASA CERES
 814 program is shown in red (<https://ceres.larc.nasa.gov/data/>, see also for example Loeb et al., 2012) for the
 815 period 2005-2018 to account for the 'golden period' of best available estimates. We obtain a total heat
 816 gain of $358 \pm 37 \text{ ZJ}$ over the period 1971-2018, which is equivalent to a heating rate (i.e. the EEI) of 0.47
 817 $\pm 0.1 \text{ Wm}^{-2}$ applied continuously over the surface area of the Earth ($5.10 \times 10^{14} \text{ m}^2$). The corresponding
 818 EEI over the period 2010-2018 amounts to $0.87 \pm 0.12 \text{ Wm}^{-2}$. A weighted least square fit has been used
 819 taking into account the uncertainty range (see also von Schuckmann and Le Traon, 2011).

820

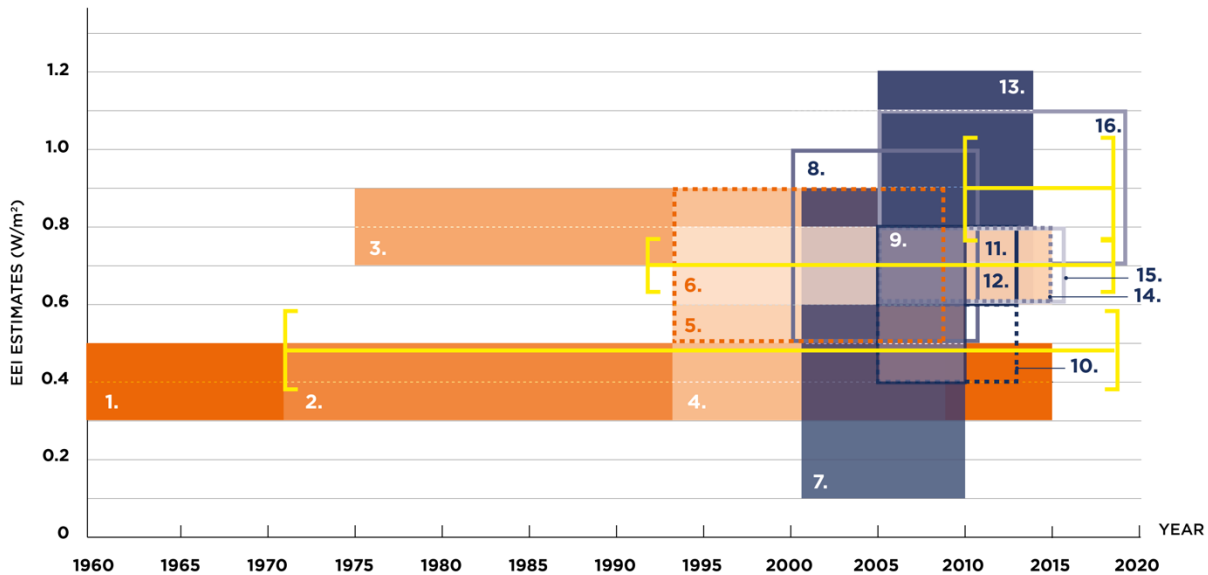
821

822 In agreement with previous studies, the Earth heat inventory based on most recent estimates of
 823 heat gain in the ocean (section 1), the atmosphere (section 2), land (section 3) and the cryosphere
 824 (section 4) shows a consistent long-term heat gain since the 1960s (Fig. 6). Our results show a total
 825 heat gain of 358 ± 37 ZJ over the period 1971-2018, which is equivalent to a heating rate of 0.47
 826 ± 0.1 Wm^{-2} , and applied continuously over the surface area of the Earth (5.10×10^{14} m^2). For
 827 comparison, the heat gain obtained in IPCC AR5 amounts to 274 ± 78 ZJ and 0.4 Wm^{-2} over the
 828 period 1971-2010 (Rhein et al., 2013). In other words, our results show that since the IPCC AR5
 829 estimate has been performed, heat accumulation has continued at a comparable rate. The major
 830 player in the Earth inventory is the ocean, particularly the upper (0-700m) and intermediate (700-
 831 2000m) ocean layers (see also section 1, Fig. 2).

832

833 Although the net flux at TOA as derived from remote sensing are anchored by an estimate of global
 834 OHC (Loeb et al., 2012), and thus does not provide a completely independent result for the total
 835 EEI, we additionally compare net flux at TOA with the Earth heat inventory obtained in this study
 836 (Fig. 6). Both rate of changes compare well, and we obtain 0.7 ± 0.1 Wm^{-2} for the remote sensing
 837 estimate at TOA, and 0.8 ± 0.1 Wm^{-2} for the Earth heat inventory over the period 2005-2018.

838



839

840 *Fig. 7: Overview on EEI estimates as obtained from previous publications, and references are listed in the*
841 *figure legend. For IPCC AR5, Rhein et al. (2013) is used. The color bars take into account the uncertainty*
842 *ranges provided in each publication, respectively. For comparison, the estimates of our Earth heat*
843 *inventory based on the results of Fig. 6 have been added (yellow lines) for the periods 1971-2018, 1993-*
844 *2018 and 2010-2018, and the trends have been evaluated using a weighted least square fit (see von*
845 *Schuckmann and Le Traon, 2011 for details on the method).*

846
847

848 Rates of change derived from Fig. 6 are in agreement with previously published results for the
849 different periods (Fig. 7). Major disagreements occur for the estimate of Balmaseda et al. (2013)
850 which is obtained from an ocean reanalysis, and known to provide higher heat gain compared to
851 results derived strictly from observations (Meyssignac et al., 2019). Over the last quarter of a
852 decade this Earth heat inventory reports - in agreement with previous publications - an increased
853 rate of Earth heat uptake reaching up to 0.9 W/m^2 (Fig. 7). This period is also characterized with
854 an increase in the availability and quality of the global climate observing system, particularly for
855 the past 2 decades. The heat inventory as obtained in this study reveals an EEI of $0.87 \pm 0.12 \text{ W/m}^2$
856 over the period 2010-2018 - a period which experienced record levels of Earth surface warming,
857 and is ranked as the warmest decade relative to the reference period 1850-1900 (WMO, 2020).
858 Whether this increased rate can be attributed to an acceleration of global warming and Earth system
859 heat uptake (e.g. Cheng et al., 2018; WMO, 2020; Blunden and Arndt, 2019), or an induced
860 estimation bias due to the interplay between natural and anthropogenic driven variability (e.g.
861 Cazenave et al., 2014), or underestimated uncertainties in the historical record (e.g. Boyer et al.,
862 2016) needs further investigation.

863

864 The new multidisciplinary estimate obtained from a concerted international effort provides an
865 updated insight in where the heat is going from a positive EEI of $0.47 \pm 0.1 \text{ W/m}^2$ for the period
866 1971-2018. Over the period 1971-2018 (2010-2018), 89% (90%) of the EEI is stored in the global
867 ocean, from which 52% (52%) is repartitioned in the upper 700m depth and 28% (30%) at
868 intermediate layers (700-2000m), and 9% (8%) in the deep ocean layer below 2000m depth.
869 Atmospheric warming amounts to 1% (2%) in the Earth heat inventory, the land heat gain with
870 6% (5%) and the heat uptake by the cryosphere with 4% (3%). These results show general
871 agreement with previous estimates (e.g. Rhein et al., 2013). Over the period 2010-2018, the EEI
872 amounts to $0.87 \pm 0.12 \text{ W/m}^2$, indicating a rapid increase in EEI over the past decade. Note that a
873 near-global (60°N - 60°S) area for the ocean heat uptake is used in this study, which could induce
874 a slight underestimation, and needs further evaluation in the future (see section 1). However, a test
875 using a single dataset (Cheng et al., 2017) indicates that the ocean contribution within 1960-2018
876 can increase by 1% if the full global ocean domain is used (not shown).

877

878

879

880

881 6. Conclusion

882

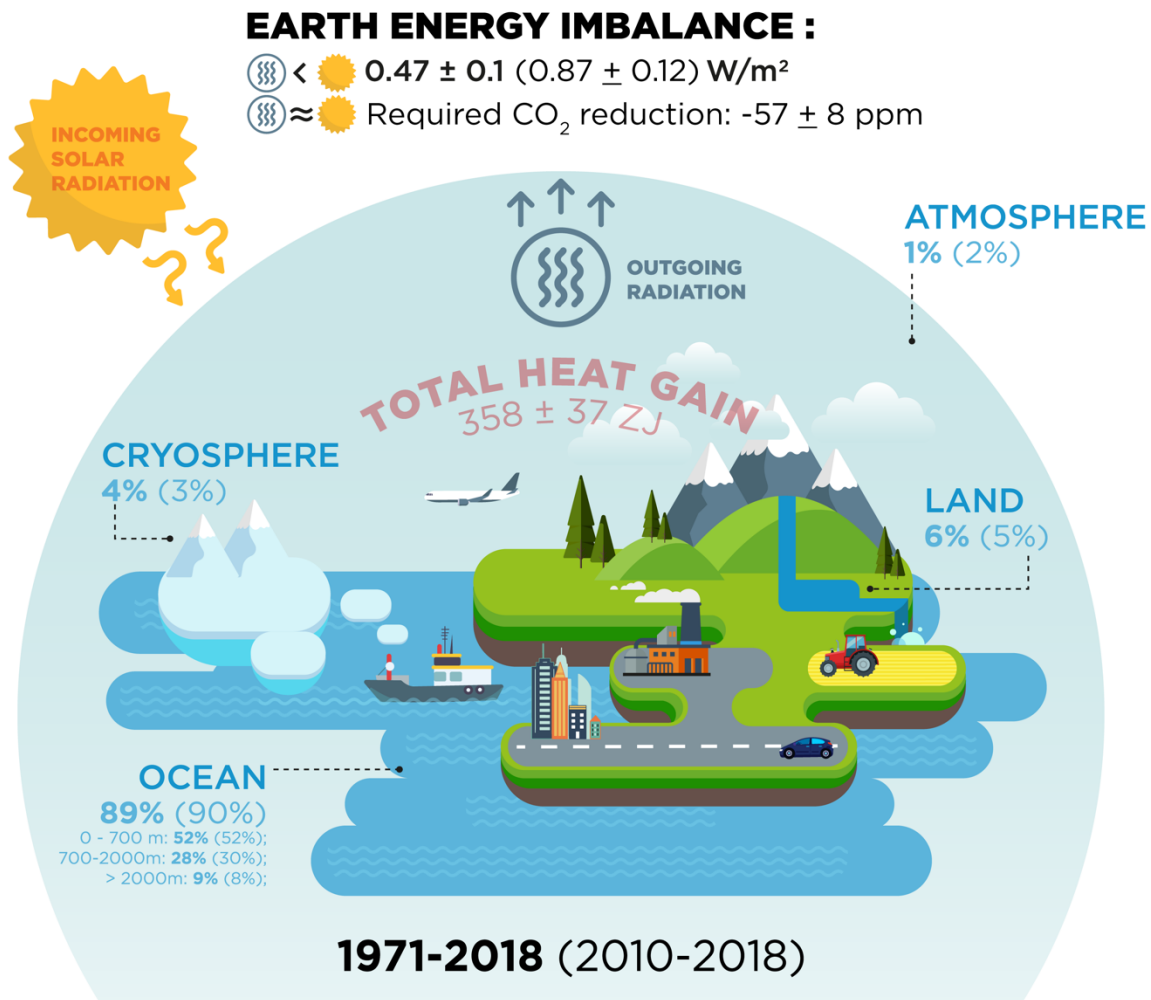
883 The UN 2030 Agenda for Sustainable Development states that climate change is “one of the
884 greatest challenges of our time...” and warns “...the survival of many societies, and of the
885 biological support systems of the planet, is at risk” (UNGA, 2015). The outcome document of the
886 Rio+20 Conference, *The Future We Want*, defines climate change as “an inevitable and urgent
887 global challenge with long-term implications for the sustainable development of all countries”
888 (UNGA, 2012). The Paris agreement builds upon the United Nations Framework Convention on
889 Climate Change (UN, 1992) and for the first time all nations agreed to undertake ambitious efforts
890 to combat climate change, with the central aim to keep global temperature rise this century well
891 below 2°C above pre-industrial levels and to limit the temperature increase even further to 1.5°C
892 (UN, 2015). Article 14 of the Paris Agreement requires the *Conference of the Parties serving as*
893 *the meeting of the Parties to the Paris Agreement* (CMA) to periodically take stock of the
894 implementation of the Paris Agreement and to assess collective progress towards achieving the
895 purpose of the Agreement and its long-term goals through the so called global stocktake based on
896 best available science.

897

898 The EEI is the most critical number defining the prospects for continued global warming and
899 climate change (Hansen et al., 2011, von Schuckmann et al., 2016), and we call for an
900 implementation of the EEI into the global stocktake. The current positive EEI is understood to be
901 foremost and primarily a result of increasing atmospheric greenhouse gases (IPCC, 2013), which
902 have - according to the IPCC special report on Global Warming of 1.5 °C - already ‘caused
903 approximately 1.0°C of global warming above pre-industrial levels, with a likely range of 0.8°C
904 to 1.2°C’ (IPCC, 2018). The IPCC special report further states with high confidence that ‘global
905 warming is likely to reach 1.5°C between 2030 and 2052 if it continues to increase at the current
906 rate’. The EEI is the portion of the forcing that the Earth’s climate system has not yet responded
907 to (Hansen et al., 2005), and defines additional global warming that will occur without further
908 change in forcing (Hansen et al., 2017). Our results show that EEI is not only continuing, it is
909 increasing. Over the period 1971-2018 average EEI amounts to $0.47 \pm 0.12 \text{ W/m}^2$, but amounts to
910 $0.87 \pm 0.12 \text{ W/m}^2$ during 2010-2018 (Fig. 8). Concurrently, acceleration of sea level rise (WCRP,
911 2018; Legelais et al., 2020), accelerated surface warming, record temperatures and sea ice loss in
912 the Arctic (Richter-Menge et al., 2019; WMO, 2020; Blunden and Arndt, 2020) and ice loss from
913 the Greenland ice sheet (King et al., 2020), and intensification of atmospheric warming near-
914 surface and in the troposphere (Steiner et al., 2020) have been - for example - recently reported.
915 To what degree these changes are intrinsically linked needs further evaluations.

916

917



918
919
920
921
922
923
924
925
926
927

Figure 8: Schematic presentation on the Earth heat inventory for the current anthropogenic driven positive Earth energy imbalance at the Top Of the Atmosphere (TOA). Relative partition (in %) of the Earth heat inventory presented in Fig. 6 for the different components are given for the ocean (upper: 0-700m, intermediate: 700-2000m, deep: > 2000m), land, cryosphere (grounded and floating ice) and atmosphere, for the periods 1971-2018 and 2010-2018 (for the latter period values are provided in parentheses), as well as for the EEI. The total heat gain (in red) over the period 1971-2018 is obtained from the Earth heat inventory as presented in Fig. 6. To reduce the 2010-2018 EEI of $0.87 \pm 0.12 \text{ W/m}^2$ to zero, current atmospheric CO_2 would need to be reduced by -57 ± 8 ppm (see text for more details).

928
929
930
931
932
933
934

Global atmospheric CO_2 concentration reached 407.38 ± 0.1 ppm averaged over 2018 (Friedlingstein et al., 2019) and 409.8 ± 0.1 ppm in 2019 (Blunden and Arndt, 2020). WMO (2020) reports CO_2 concentrations at the Mauna Loa measurement platform of 411.75 ppm in February 2019, and 414.11 ppm in February 2020. Stabilization of climate, the goal of the universally agreed UNFCCC (UN, 1992) and the Paris Agreement (UN, 2015), requires that EEI be reduced to approximately zero to achieve Earth's system quasi-equilibrium. The change of heat radiation to space for a given greenhouse gas change can be computed accurately. The amount of CO_2 in the

935 atmosphere would need to be reduced from 410 ppm to 353 ppm (i.e. a required reduction of -57
936 ± 8 ppm) to increase heat radiation to space by 0.87 W/m^2 , bringing Earth back towards energy
937 balance (Fig. 8), where we have used the analytic formulae of Hansen et al. (2000) for this
938 estimation. Atmospheric CO_2 was last 350 ppm in the year 1988, and global Earth's surface
939 temperature was then $+0.5^\circ\text{C}$ relative to the pre-industrial period (relative to the 1880-1920 mean)
940 (Hansen et al., 2017; Friedlingstein et al., 2019). In principle, we could reduce other greenhouse
941 gases, and thus require a less stringent reduction of CO_2 . However, as discussed by Hansen et al.
942 (2017), some continuing increase of N_2O , whose emissions are associated with food production,
943 seems inevitable, so there is little prospect for much net reduction of non- CO_2 greenhouse gases,
944 and thus, the main burden for climate stabilization falls on CO_2 reduction. This simple number,
945 EEI, is the most fundamental metric that the scientific community and public must be aware of, as
946 the measure of how well the world is doing in the task of bringing climate change under control
947 (Fig. 8).

948

949 This community effort also addresses gaps for the evolution of future observing systems for a
950 robust and continued assessment of the Earth heat inventory, and its different components.
951 Immediate priorities include the maintenance and extension of the global climate observing system
952 to assure a continuous monitoring of the Earth heat inventory, and to reduce the uncertainties. For
953 the global ocean observing system, the core Argo sampling needs to be sustained, and
954 complemented by remote sensing data. Extensions such as into the deep ocean layer need to be
955 further fostered (Desbruyères et al., 2017; Johnson et al., 2015), and technical developments for
956 the measurements under ice and in shallower areas need to be sustained and extended. Moreover,
957 continued efforts are needed to further advance bias correction methodologies, uncertainty
958 evaluations and data processing of the historical dataset.

959

960 In order to allow for improvements on the present estimates of changes in the continental heat and
961 to ensure that the database is continued into the future, an international, coordinated effort is
962 needed to increase the number of subsurface temperature data from BTPs at additional locations
963 around the world, in particular in the southern hemisphere. Additionally, repeated monitoring
964 (after a few decades) of existing boreholes should help reduce uncertainties at individual sites.
965 Such data should be shared through an open platform.

966

967 For the atmosphere, the continuation of operational satellite- and ground-based observations is
968 important but the foremost need is sustaining and enhancing a coherent long-term monitoring
969 system for the provision of climate data records of essential climate variables. GNSS radio
970 occultation observations and reference radiosonde stations within the Global Climate Observing
971 System (GCOS) Reference Upper Air Network (GRUAN) are regarded as climate benchmark
972 observations. Operational radio occultation missions for continuous global climate observations
973 need to be maintained and expanded, ensuring global coverage over all local times, as the central
974 node of a global climate observing system.

975
976 For the cryosphere, sustained remote sensing for all of the cryosphere components is key to
977 quantifying future changes over these vast and inaccessible regions, but must be complemented by
978 in-situ observations for calibration and validation. For sea-ice, the albedo, the area and ice
979 thickness are all essential, with ice-thickness being particularly challenging to quantify with
980 remote sensing alone. For ice sheets and glaciers, reliable gravimetric measurements, ice thickness
981 and extent, snow/firn thickness and density are essential to quantify changes in mass balance of
982 grounded and floating ice. We highlight Antarctic sea-ice change and warming of firn as terms
983 that are poorly constrained or have not significantly contributed to this assessment but may become
984 important over the coming decades. Similarly, there exists the possibility for rapid change
985 associated with positive ice dynamical feedbacks at the marine margins of the Greenland and
986 Antarctic ice sheets. Sustained monitoring of each of these components will, therefore, serve the
987 dual purpose of furthering understanding of the dynamics and quantifying the contribution to
988 Earth's energy budget. In addition to data collection, open access to the data and data synthesis
989 products as well as coordinated international efforts are key to the continued monitoring of the ice
990 loss from the cryosphere and related energy uptake.

991
992 Sustained and improved observations to quantify Earth's changing energy inventory are also
993 critical to the development of improved physical models of the climate system, including both data
994 assimilation efforts that help us to understand past changes and predictions (Storto et al., 2019)
995 and climate models used to provide projections of future climate change (Eyring et al., 2019). For
996 example, atmospheric reanalyses have shown to be a valuable tool for investigating past changes
997 in the EEI (Allan et al., 2014) and ocean reanalyses have proven useful in estimating rates of ocean
998 heating on annual and sub-annual timescales by reducing observational noise (Trenberth et al.,
999 2016). Furthermore, both reanalyses and climate models can provide information to assess current
1000 observing capabilities (Fujii et al., 2019) and improve uncertainty estimates in the different
1001 components of Earth's energy inventory (Allison et al., 2019). Future priorities for expanding the
1002 observing system to improve future estimates of EEI should be cognizant of the expected evolution
1003 of the climate change signal, drawing on evidence from observations, models and theory
1004 (Meysignac et al., 2019; Palmer et al., 2019).

1005
1006 A continuous effort to regularly update the Earth heat inventory is important to quantify how much
1007 and where heat accumulated from climate change is stored in the climate system. The Earth heat
1008 inventory crosses multi-disciplinary boundaries, and calls for the inclusion of new science
1009 knowledge from the different disciplines involved, including the evolution of climate observing
1010 systems and associated data products, uncertainty evaluations and processing tools. The results
1011 provide indications that a redistribution and conversion of energy in the form of heat is taking
1012 place in the different components of the Earth system, particularly within the ocean, and that EEI
1013 has increased over the past decade. The outcomes have further demonstrated how we are able to
1014 evolve our estimates for the Earth heat inventory while bringing together different expertise and

1015 major climate science advancements through a concerted international effort. All of these
1016 component estimates are at the leading edge of climate science. Their union has provided a new
1017 and unique insight on the inventory of heat in the Earth system, its evolution over time, as well as
1018 a revision of the absolute values. The data product of this effort is made available and can be thus
1019 used for model validation purposes.

1020
1021 This study has demonstrated the unique value of such a concerted international effort, and we thus
1022 call for a regular evaluation of the Earth heat inventory. This first attempt presented here has been
1023 focused on the global area average only, and evolving into regional heat storage and redistribution,
1024 the inclusion of various time-scales (e.g. seasonal, year-to-year), and other climate study tools (e.g.
1025 indirect methods, ocean reanalyses) would be an important asset of this much needed regular
1026 international framework for the Earth heat inventory. This would also respond directly to the
1027 request of GCOS to establish the observational requirements needed to monitor the Earth's cycles
1028 and the global energy budget. The outcome of this study will therefore directly feed into GCOS'
1029 assessment of the status of the global climate observing system due in 2021 which is the basis for
1030 the next implementation plan. These identified observation requirements will guide the
1031 development of the next generation of in-situ and satellite global climate observations by all
1032 national meteorological services and space agencies and other oceanic and terrestrial networks.

1033
1034
1035
1036 **Data availability:** The time series of the Earth heat inventory are published at DKRZ
1037 (<https://www.dkrz.de/>) under the doi: https://doi.org/10.26050/WDCC/GCOS_EHI_EXP_v2 (von
1038 Schuckmann et al., 2020). The data contain an updated international assessment of ocean warming
1039 estimates, and new and updated estimates of heat gain in the atmosphere, cryosphere and land over
1040 the period 1960-2018. This published dataset has been used to build the basis for Figure 6 of this
1041 manuscript. The ocean warming estimate is based on an international assessment of 15 different
1042 in situ data-based ocean products as presented in section 1. The new estimate of the atmospheric
1043 heat content is fully described in section 2, and is backboneed on a combined use of atmospheric
1044 reanalyses, multi-satellite data and radiosonde records, and microwave sounding techniques. The
1045 land heat storage time series as presented in section 3 relies on borehole data. The heat available
1046 to account for cryosphere loss is presented in section 4, and is based on a combined use of model
1047 results and observations to obtain estimates of major cryosphere components such as polar ice
1048 sheets, Arctic sea-ice and glaciers.

1049
1050
1051
1052
1053
1054

1055

1056 **GCOS Earth heat inventory team: Author contributions**

1057

1058 Coordination: Karina von Schuckmann¹, Lijing Cheng^{2,28}, Matthew D. Palmer³, Caterina
1059 Tassone⁵, Valentin Aich⁵

1060

1061 Ocean: Karina von Schuckmann¹, Lijing Cheng^{2,28}, Tim Boyer⁸, Damien Desbruyères⁹, Catia
1062 Domingues^{10,11}, John Gilson¹³, Masayoshi Ishii¹⁶, Gregory C. Johnson¹⁷, Rachel E. Killick³, Brian
1063 A. King¹⁰, Nicolas Kolodziejczyk¹⁸, John Lyman¹⁷, Maeva Monier²⁰, Didier Paolo Monselesan²¹,
1064 Sarah Purkey⁶, Dean Roemmich⁶, Susan E. Wijffels^{21,26}

1065

1066 Atmosphere: Gottfried Kirchengast¹⁴, Maximilian Gorfer¹⁴, Andrea K. Steiner¹⁴, Michael
1067 Mayer^{15,29}, Leopold Haimberger¹⁵

1068

1069 Land: Almudena García-García⁷, Francisco José Cuesta-Valero^{7,27}, Hugo Beltrami⁷, Sonia I.
1070 Seneviratne²³, Pierre Gentine¹²

1071

1072 Cryosphere: Fiammetta Straneo⁶, Susheel Adusumilli⁶, Donald A. Slater⁶, Mary-Louise
1073 Timmermans²⁵, Ben Marzeion¹⁹, Axel Schweiger²², Andrew Shepherd²⁴

1074

1075 Earth energy inventory: all authors, with specific contributions from Karina von Schuckmann¹,
1076 Almudena García-García⁷, Francisco José Cuesta-Valero^{7,27}, James Hansen⁴, Maeva Monier¹⁹

1077

1078 Conclusion: all authors, with specific contributions from Karina von Schuckmann¹, James
1079 Hansen⁴, Caterina Tassone⁵, Valentin Aich⁵, Lijing Cheng^{2,28}, Matthew D. Palmer³, Gottfried
1080 Kirchengast¹⁴, Andrea K. Steiner¹⁴, Almudena García-García⁷, Francisco José Cuesta-Valero^{7,27},
1081 Hugo Beltrami⁷, Fiammetta Straneo⁶

1082

1083 ¹Mercator Ocean International, France

1084 ²Institute of Atmospheric Physics, Chinese Academy of Sciences, China

1085 ³Met Office Hadley Centre, UK

1086 ⁴Columbia University Earth Institute, USA

1087 ⁵WMO/GCOS, Switzerland

1088 ⁶Scripps Institution of Oceanography, UCSD, San Diego, CA, USA

1089 ⁷Climate & Atmospheric Sciences Institute, St. Francis Xavier University, NS, Canada

1090 ⁸NOAA's National Centers for Environmental Information

1091 ⁹Ifremer, University of Brest, CNRS, IRD, Laboratoire d'Océanographie Physique et Spatiale, France

1092 ¹⁰National Oceanographic Centre, UK

1093 ¹¹ARC Centre of Excellence for Climate Extremes, University of Tasmania, Hobart, Tasmania, Australia

1094 ¹²Earth and Environmental Engineering in the School of Engineering and Applied Sciences, Columbia University,
1095 USA

1096 ¹³University of California, USA

1097 ¹⁴Wegener Center for Climate and Global Change and Institute of Physics, University of Graz, Austria

- 1098 ¹⁵Department of Meteorology and Geophysics, University of Vienna, Austria
1099 ¹⁶Department of Atmosphere, Ocean and Earth System Modeling Research, Meteorological Research Institute, Japan
1100 ¹⁷NOAA, Pacific Marine Environmental Laboratory, USA
1101 ¹⁸University of Brest, CNRS, IRD, Ifremer, Laboratoire d'Océanographie Physique et Spatiale, IUEM, France
1102 ¹⁹Institute of Geography and MARUM-Center for Marine Environmental Sciences, University of Bremen, Germany
1103 ²⁰CELAD/Mercator Ocean International, France
1104 ²¹CSIRO Oceans and Atmosphere, Hobart, Tasmania, Australia
1105 ²²Polar Science Center, Applied Physics Laboratory, University of Washington, Seattle, USA
1106 ²³Institute for Atmospheric and Climate Science, ETH, Switzerland
1107 ²⁴Center for Polar Observation and Modeling, University of Leeds, UK
1108 ²⁵Department of Earth and Planetary Sciences, Yale University, New Haven, USA
1109 ²⁶Woods Hole Oceanographic Institution, Massachusetts, United States
1110 ²⁷Environmental Sciences Program, Memorial University of Newfoundland, NL, Canada
1111 ²⁸Center for Ocean Mega-Science, Chinese Academy of Sciences, Qingdao, China, 266071
1112 ²⁹European Centre for Medium-Range Weather Forecasts, Reading, UK

1113

1114 **Acknowledgements:**

1115

1116 This research benefited from long-term attention by GCOS and builds on initial work carried out under the
1117 WCRP core projects CLIVAR, GEWEX, CliC and SPARC.

1118

1119 MDP and REK were supported by the Met Office Hadley Centre Climate Programme funded by the BEIS
1120 and Defra.

1121

1122 Ocean: PMEL contribution number 5053; Funding: CMD was supported by an ARC Future Fellowship
1123 (FT130101532). L.Cheng is supported by Key Deployment Project of Centre for Ocean Mega-Research of
1124 Science, CAS (COMS2019Q01).

1125

1126 Atmosphere: The authors express their gratitude to SPARC for supporting this activity under sponsorship
1127 of the WCRP. M. Gorfer was supported by WEGC atmospheric remote sensing and climate system research
1128 group young scientist funds. M. Mayer was supported by Austrian Science Fund project P33177. We
1129 acknowledge the WEGC EOPAC team for providing the OPSv5.6 RO data (available online at
1130 <https://doi.org/10.25364/WEGC/OPS5.6:2019.1>) as well as quality-processed Vaisala RS data,
1131 UCAR/CDAAC (Boulder, CO, USA) for access to RO phase and orbit data, RSS (Santa Rosa, CA, USA)
1132 for providing MSU V4.0 data, ECMWF (Reading, UK) for access to operational analysis and forecast data,
1133 ERA5 reanalysis data, and RS data from the ERA-Interim archive, JMA (Tokyo, Japan) for provision of
1134 the JRA55 and JRA55C reanalysis data, and NASA GMAO (Greenbelt, MD, USA) for access of the
1135 MERRA-2 reanalysis data.

1136

1137 Land: This work was supported by grants from the National Sciences and Engineering Research Council
1138 of Canada Discovery Grant (NSERC DG 140576948) and the Canada Research Chairs Program (CRC
1139 230687) to H. Beltrami. Almudena García-García and Francisco José Cuesta-Valero are funded by
1140 Beltrami's CRC program, the School of Graduate Studies at Memorial University of Newfoundland and
1141 the Research Office at St. Francis Xavier University

1142

1143 Ice: This work was supported by CliC (Climate and Cryosphere Project of the World Climate Research
1144 Program). FS acknowledges support by NSF OCE 1657601. SA was supported by the NASA grant
1145 80NSSC18K1424.

1146
1147 We also would like to thank Marianne Nail (<https://girlsmakesense.com/>) for her support to the graphical
1148 development of Fig. 7 and 8.

1149
1150

1151

1152 References

- 1153 Abraham, J. P., Baringer, M., Bindoff, N. L., Boyer, T., Cheng, L. J., Church, J. A., Conroy, J. L., Domingues, C.
1154 M., Fasullo, J. T., Gilson, J., Goni, G., Good, S. A., Gorman, J. M., Gouretski, V., Ishii, M., Johnson, G. C.,
1155 Kizu, S., Lyman, J. M., Macdonald, A. M., ... Willis, J. K. (2013). A review of global ocean temperature
1156 observations: Implications for ocean heat content estimates and climate change. *Reviews of Geophysics*, *51*(3),
1157 450–483. <https://doi.org/10.1002/rog.20022>
- 1158 Adusumilli, S., Fricker, H. A., Medley, B., Padman, L., & Siegfried, M. R. (2019). Multi-year variability in ocean-
1159 driven melting of Antarctica's ice shelves. *Nature Geoscience*, under review.
- 1160 Allan, R. P., Liu, C., Loeb, N. G., Palmer, M. D., Roberts, M., Smith, D., & Vidale, P.-L. (2014). Changes in global
1161 net radiative imbalance 1985-2012 (I10, trans.). *Geophysical Research Letters*, *41*(15), 5588–5597.
1162 <https://doi.org/10.1002/2014GL060962>
- 1163 Allison, L. C., Roberts, C. D., Palmer, M. D., Hermanson, L., Killick, R. E., Rayner, N. A., Smith, D. M., &
1164 Andrews, M. B. (2019). Towards quantifying uncertainty in ocean heat content changes using synthetic
1165 profiles. *Environmental Research Letters*, *14*(8), 084037. <https://doi.org/10.1088/1748-9326/ab2b0b>
- 1166 Angerer, B., Ladstädter, F., Scherllin-Pirscher, B., Schwärz, M., Steiner, A. K., Foelsche, U., & Kirchengast, G.
1167 (2017). Quality aspects of the Wegener Center multi-satellite GPS radio occultation record OPSv5.6. *Atmos.*
1168 *Meas. Tech.*, *10*(12), 4845–4863. <https://doi.org/10.5194/amt-10-4845-2017>
- 1169 Baggenstos, D., Häberli, M., Schmitt, J., Shackleton, S. A., Birner, B., Severinghaus, J. P., Kellerhals, T., & Fischer,
1170 H. (2019). Earth's radiative imbalance from the Last Glacial Maximum to the present. *Proceedings of the*
1171 *National Academy of Sciences*, *116*(30), 14881. <https://doi.org/10.1073/pnas.1905447116>
- 1172 Bailey, V. L., Pries, C. H., & Lajtha, K. (2019). What do we know about soil carbon destabilization? *Environmental*
1173 *Research Letters*, *14*(8), 083004. <https://doi.org/10.1088/1748-9326/ab2c11>
- 1174 Bamber, J. L., Westaway, R. M., Marzeion, B., & Wouters, B. (2018). The land ice contribution to sea level during
1175 the satellite era. *Environmental Research Letters*, *13*(6), 063008. <https://doi.org/10.1088/1748-9326/aac2f0>
- 1176 Barkaoui, A. E., Correia, A., Zarhloule, Y., Rimi, A., Carneiro, J., Boughriba, M., & Verdoya, M. (2013).
1177 Reconstruction of remote climate change from borehole temperature measurement in the eastern part of
1178 Morocco. *Climatic Change*, *118*(2), 431–441. <https://doi.org/10.1007/s10584-012-0638-7>
- 1179 Beck, A. E. (1977). Climatically perturbed temperature gradients and their effect on regional and continental heat-
1180 flow means. *Tectonophysics*, *41*(1), 17–39. [https://doi.org/https://doi.org/10.1016/0040-1951\(77\)90178-0](https://doi.org/https://doi.org/10.1016/0040-1951(77)90178-0)
- 1181 Beltrami, H. (2001). Surface heat flux histories from inversion of geothermal data: Energy balance at the Earth's
1182 surface. *Journal of Geophysical Research: Solid Earth*, *106*(B10), 21979–21993.
1183 <https://doi.org/10.1029/2000JB000065>
- 1184 Beltrami, H. (2002a). Earth's Long-Term Memory. *Science*, *297*(5579), 206.
1185 <https://doi.org/10.1126/science.1074027>
- 1186 Beltrami, H. (2002b). Climate from borehole data: Energy fluxes and temperatures since 1500. *Geophysical*
1187 *Research Letters*, *29*(23), 26-1-26–4. <https://doi.org/10.1029/2002GL015702>
- 1188 Beltrami, H., & Boulron, E. (2004). Ground warming patterns in the Northern Hemisphere during the last five
1189 centuries. *Earth and Planetary Science Letters*, *227*(3), 169–177.
1190 <https://doi.org/https://doi.org/10.1016/j.epsl.2004.09.014>
- 1191 Beltrami, H., Boulron, E., Kellman, L., & González-Rouco, J. F. (2006). Spatial patterns of ground heat gain in the
1192 Northern Hemisphere. *Geophysical Research Letters*, *33*(6). <https://doi.org/10.1029/2006GL025676>
- 1193 Beltrami, H., Matharoo, G. S., & Smerdon, J. E. (2015). Impact of borehole depths on reconstructed estimates of

1194 ground surface temperature histories and energy storage. *Journal of Geophysical Research: Earth Surface*,
1195 120(5), 763–778. <https://doi.org/10.1002/2014JF003382>

1196 Beltrami, H., Matharoo, G. S., Smerdon, J. E., Illanes, L., & Tarasov, L. (2017). Impacts of the Last Glacial Cycle
1197 on ground surface temperature reconstructions over the last millennium. *Geophysical Research Letters*, 44(1),
1198 355–364. <https://doi.org/10.1002/2016GL071317>

1199 Beltrami, H., Smerdon, J. E., Pollack, H. N., & Huang, S. (2002). Continental heat gain in the global climate system.
1200 *Geophysical Research Letters*, 29(8), 8-1-8–3. <https://doi.org/10.1029/2001GL014310>

1201 Bense, V. F., & Kooi, H. (2004). Temporal and spatial variations of shallow subsurface temperature as a record of
1202 lateral variations in groundwater flow. *Journal of Geophysical Research: Solid Earth*, 109(B4).
1203 <https://doi.org/10.1029/2003JB002782>

1204 Berrisford, P., Kållberg, P., Kobayashi, S., Dee, D., Uppala, S., Simmons, A. J., Poli, P., & Sato, H. (2011).
1205 Atmospheric conservation properties in ERA-Interim. *Quarterly Journal of the Royal Meteorological Society*,
1206 137(659), 1381–1399. <https://doi.org/10.1002/qj.864>

1207 Bindoff, N. L., Cheung, W. W. L., & Kairo, J. G. (2019). Changing Ocean, Marine Ecosystems, and Dependent
1208 Communities. In H. O. Pörtner, D. C. Roberts, V. Masson-Delmotte, P. Zhai, M. Tignor, E. Poloczanska, K.
1209 Mintenbeck, A. Alegria, M. Nicolai, A. Okem, J. Petzold, B. Rama, & N. M. Weyer (Eds.), *Special Report:
1210 The Ocean and Cryosphere in a Changing Climate Summary for Policymakers* (pp. 447–587). in press.
1211 <https://doi.org/https://www.ipcc.ch/report/srocc/>

1212 Blunden, J. and Arndt, D. S. (2019). State of the Climate in 2019. Bulletin of the American Meteorological Society,
1213 100(9), Si–S305, doi:10.1175/2019BAMSStateoftheClimate.1.

1214 Blunden, J. and D. S. Arndt, Eds., 2020: State of the Climate in 2019. Bull. Amer. Meteor. Soc.,
1215 101 (8), Si–S429 <https://doi.org/10.1175/2020BAMSStateoftheClimate.1>

1216 Bopp, L., Resplandy, L., Orr, J. C., Doney, S. C., Dunne, J. P., Gehlen, M., Halloran, P., Heinze, C., Ilyina, T.,
1217 Séférian, R., Tjiputra, J., & Vichi, M. (2013). Multiple stressors of ocean ecosystems in the 21st century:
1218 projections with CMIP5 models. *Biogeosciences*, 10(10), 6225–6245. <https://doi.org/10.5194/bg-10-6225-2013>

1219 Boyer, T., Domingues, C. M., Good, S. A., Johnson, G. C., Lyman, J. M., Ishii, M., Gouretski, V., Willis, J. K.,
1220 Antonov, J., Wijffels, S., Church, J. A., Cowley, R., & Bindoff, N. L. (2016). Sensitivity of Global Upper-
1221 Ocean Heat Content Estimates to Mapping Methods, XBT Bias Corrections, and Baseline Climatologies.
1222 *Journal of Climate*, 29(13), 4817–4842. <https://doi.org/10.1175/JCLI-D-15-0801.1>

1223 Breitburg, D., Levin, L. A., Oschlies, A., Grégoire, M., Chavez, F. P., Conley, D. J., Garçon, V., Gilbert, D.,
1224 Gutiérrez, D., Isensee, K., Jacinto, G. S., Limburg, K. E., Montes, I., Naqvi, S. W. A., Pitcher, G. C., Rabalais,
1225 N. N., Roman, M. R., Rose, K. A., Seibel, B. A., ... Zhang, J. (2018). Declining oxygen in the global ocean
1226 and coastal waters. *Science*, 359(6371), eaam7240. <https://doi.org/10.1126/science.aam7240>

1227 Cabanes, C., Grouazel, A., Von Schuckmann, K., Hamon, M., Turpin, V., Coatanoan, C., Paris, F., Guinehut, S.,
1228 Boone, C., Ferry, N., De Boyer Montégut, C., Carval, T., Reverdin, G., Pouliquen, S., & Le Traon, P. Y.
1229 (2013). The CORA dataset: Validation and diagnostics of in-situ ocean temperature and salinity
1230 measurements. *Ocean Science*, 9(1), 1–18. <https://doi.org/10.5194/os-9-1-2013>

1231 Cermak, V. (1971). Underground temperature and inferred climatic temperature of the past millenium.
1232 *Palaeogeography, Palaeoclimatology, Palaeoecology*, 10(1), 1–19. [https://doi.org/10.1016/0031-0182\(71\)90043-5](https://doi.org/10.1016/0031-0182(71)90043-5)

1233 Cheng, L., Trenberth, K., Fasullo, J., Boyer, T., Abraham, J., von Schuckmann, K., & Zhou, J. (2017). Taking the
1234 Pulse of the Planet. *Eos, Transactions American Geophysical Union*, 98(1).
1235 <https://doi.org/10.1029/2017EO081839>

1236 Cheng, L., Trenberth, K. E., Palmer, M. D., Zhu, J., & Abraham, J. P. (2016). Observed and simulated full-depth
1237 ocean heat-content changes for 1970–2005. *Ocean Sci.*, 12(4), 925–935. <https://doi.org/10.5194/os-12-925-2016>

1238 Cheng, L., Trenberth, K. E., Fasullo, J., Boyer, T., Abraham, J., & Zhu, J. (2017). Improved estimates of ocean
1239 heat content from 1960 to 2015. *Science Advances*, 3(3), e1601545. <https://doi.org/10.1126/sciadv.1601545>

1240 Cheng, L., Trenberth, K. E., Fasullo, J. T., Mayer, M., Balmaseda, M., & Zhu, J. (2019). Evolution of ocean heat
1241 content related to ENSO. *Journal of Climate*, 32(12), 3529–3556. <https://doi.org/10.1175/JCLI-D-18-0607.1>

1242 Chiodo, G., & Haimberger, L. (2010). Interannual changes in mass consistent energy budgets from ERA-Interim and
1243 satellite data. *Journal of Geophysical Research: Atmospheres*, 115(D2).
1244 <https://doi.org/10.1029/2009JD012049>

- 1250 Chouinard, C., & Mareschal, J.-C. (2007). Selection of borehole temperature depth profiles for regional climate
 1251 reconstructions. *Clim. Past*, 3(2), 297–313. <https://doi.org/10.5194/cp-3-297-2007>
- 1252 Chouinard, Christian, & Mareschal, J.-C. (2009). Ground surface temperature history in southern Canada:
 1253 Temperatures at the base of the Laurentide ice sheet and during the Holocene. *Earth and Planetary Science*
 1254 *Letters*, 277(1–2), 280–289. <https://doi.org/10.1016/j.epsl.2008.10.026>
- 1255 Ciais, P., Sabine, C., Bala, G., Bopp, L., Brovkin, V., Canadell, J., Chhabra, A., DeFries, R., Galloway, J., Heimann,
 1256 M., Jones, C., Quéré, C. Le, Myneni, R. B., Piao, S., & Thornton, P. (2013). The physical science basis.
 1257 Contribution of working group I to the fifth assessment report of the intergovernmental panel on climate
 1258 change. *Change, IPCC Climate*, 465–570. <https://doi.org/10.1017/CBO9781107415324.015>
- 1259 Clark, P. U., Shakun, J. D., Marcott, S. A., Mix, A. C., Eby, M., Kulp, S., Levermann, A., Milne, G. A., Pfister, P.
 1260 L., Santer, B. D., Schrag, D. P., Solomon, S., Stocker, T. F., Strauss, B. H., Weaver, A. J., Winkelmann, R.,
 1261 Archer, D., Bard, E., Goldner, A., ... Plattner, G.-K. (2016). Consequences of twenty-first-century policy for
 1262 multi-millennial climate and sea-level change. *Nature Climate Change*, 6(4), 360–369.
 1263 <https://doi.org/10.1038/nclimate2923>
- 1264 Cohen, J., Screen, J. A., Furtado, J. C., Barlow, M., Whittleston, D., Coumou, D., Francis, J., Dethloff, K.,
 1265 Entekhabi, D., Overland, J., & Jones, J. (2014). Recent Arctic amplification and extreme mid-latitude weather.
 1266 *Nature Geoscience*, 7(9), 627–637. <https://doi.org/10.1038/ngeo2234>
- 1267 Cook, A. J., & Vaughan, D. G. (2010). Overview of areal changes of the ice shelves on the Antarctic Peninsula over
 1268 the past 50 years. *The Cryosphere*, 4(1), 77–98. <https://doi.org/10.5194/tc-4-77-2010>
- 1269 Coumou, D., Di Capua, G., Vavrus, S., Wang, L., & Wang, S. (2018). The influence of Arctic amplification on mid-
 1270 latitude summer circulation. *Nature Communications*, 9(1), 2959. <https://doi.org/10.1038/s41467-018-05256-8>
- 1271 Cuesta-Valero, F J, García-García, A., Beltrami, H., González-Rouco, J. F., & García-Bustamante, E. (2020). Long-
 1272 Term Global Ground Heat Flux and Continental Heat Storage from Geothermal Data. *Clim. Past Discuss.*,
 1273 2020, 1–27. <https://doi.org/10.5194/cp-2020-65>
- 1274 Cuesta-Valero, F J, García-García, A., Beltrami, H., Zorita, E., & Jaume-Santero, F. (2019). Long-term Surface
 1275 Temperature (LoST) database as a complement for GCM preindustrial simulations. *Clim. Past*, 15(3), 1099–
 1276 1111. <https://doi.org/10.5194/cp-15-1099-2019>
- 1277 Cuesta-Valero, Francisco José, García-García, A., Beltrami, H., & Smerdon, J. E. (2016). First assessment of
 1278 continental energy storage in CMIP5 simulations. *Geophysical Research Letters*, 43(10), 5326–5335.
 1279 <https://doi.org/10.1002/2016GL068496>
- 1280 Davis, M. G., Harris, R. N., & Chapman, D. S. (2010). Repeat temperature measurements in boreholes from
 1281 northwestern Utah link ground and air temperature changes at the decadal time scale. *Journal of Geophysical*
 1282 *Research: Solid Earth*, 115(B5). <https://doi.org/10.1029/2009JB006875>
- 1283 Demezkhko, D. Y., & Gornostaeva, A. A. (2015). Late Pleistocene–Holocene ground surface heat flux changes
 1284 reconstructed from borehole temperature data (the Urals, Russia). *Clim. Past*, 11(4), 647–652.
 1285 <https://doi.org/10.5194/cp-11-647-2015>
- 1286 Desbruyères, D. G., Purkey, S. G., McDonagh, E. L., Johnson, G. C., & King, B. A. (2016). Deep and abyssal ocean
 1287 warming from 35 years of repeat hydrography. *Geophysical Research Letters*, 43(19), 10, 310–356, 365.
 1288 <https://doi.org/10.1002/2016GL070413>
- 1289 Desbruyères, D., McDonagh, E. L., King, B. A., & Thierry, V. (2017). Global and Full-Depth Ocean Temperature
 1290 Trends during the Early Twenty-First Century from Argo and Repeat Hydrography. *Journal of Climate*, 30(6),
 1291 1985–1997. <https://doi.org/10.1175/JCLI-D-16-0396.1>
- 1292 Dieng, H. B., Cazenave, A., Meyssignac, B., & Ablain, M. (2017). New estimate of the current rate of sea level rise
 1293 from a sea level budget approach. *Geophysical Research Letters*, 44(8), 3744–3751.
 1294 <https://doi.org/10.1002/2017GL073308>
- 1295 Eyring, V., Cox, P. M., Flato, G. M., Gleckler, P. J., Abramowitz, G., Caldwell, P., Collins, W. D., Gier, B. K., Hall,
 1296 A. D., Hoffman, F. M., Hurtt, G. C., Jahn, A., Jones, C. D., Klein, S. A., Krasting, J. P., Kwiatkowski, L.,
 1297 Lorenz, R., Maloney, E., Meehl, G. A., ... Williamson, M. S. (2019). Taking climate model evaluation to the
 1298 next level. *Nature Climate Change*, 9(2), 102–110. <https://doi.org/10.1038/s41558-018-0355-y>
- 1299 Fischer, E. M., & Knutti, R. (2016). Observed heavy precipitation increase confirms theory and early models.
 1300 *Nature Climate Change*, 6(11), 986–991. <https://doi.org/10.1038/nclimate3110>
- 1301 Friedlingstein, P., Jones, M. W., O'Sullivan, M., Andrew, R. M., Hauck, J., Peters, G. P., Peters, W., Pongratz, J.,
 1302 Sitch, S., Le Quéré, C., Bakker, D. C. E., Canadell, J. G., Ciais, P., Jackson, R. B., Anthoni, P., Barbero, L.,
 1303 Bastos, A., Bastrikov, V., Becker, M., Bopp, L., Buitenhuis, E., Chandra, N., Chevallier, F., Chini, L. P.,
 1304 Currie, K. I., Feely, R. A., Gehlen, M., Gilfillan, D., Gkritzalis, T., Goll, D. S., Gruber, N., Gutekunst, S.,
 1305 Harris, I., Haverd, V., Houghton, R. A., Hurtt, G., Ilyina, T., Jain, A. K., Joetzjer, E., Kaplan, J. O., Kato, E.,

1306 Klein Goldewijk, K., Korsbakken, J. I., Landschützer, P., Lauvset, S. K., Lefèvre, N., Lenton, A., Lienert, S.,
1307 Lombardozzi, D., Marland, G., McGuire, P. C., Melton, J. R., Metzl, N., Munro, D. R., Nabel, J. E. M. S.,
1308 Nakaoka, S.-I., Neill, C., Omar, A. M., Ono, T., Peregón, A., Pierrot, D., Poulter, B., Rehder, G., Resplandy,
1309 L., Robertson, E., Rödenbeck, C., Séférian, R., Schwinger, J., Smith, N., Tans, P. P., Tian, H., Tilbrook, B.,
1310 Tubiello, F. N., van der Werf, G. R., Wiltshire, A. J., and Zaehle, S.: Global Carbon Budget 2019, *Earth Syst.*
1311 *Sci. Data*, 11, 1783–1838, <https://doi.org/10.5194/essd-11-1783-2019>, 2019.

1312 Frölicher, T. L., Fischer, E. M., & Gruber, N. (2018). Marine heatwaves under global warming. *Nature*, 560(7718),
1313 360–364. <https://doi.org/10.1038/s41586-018-0383-9>

1314 Fu, Q., Solomon, S., Pahlavan, H. A., & Lin, P. (2019). Observed changes in Brewer–Dobson circulation for 1980–
1315 2018. *Environmental Research Letters*, 14(11), 114026. <https://doi.org/10.1088/1748-9326/ab4de7>

1316 Fujii, Y., Rémy, E., Zuo, H., Oke, P., Halliwell, G., Gasparin, F., Benkiran, M., Loose, N., Cummings, J., Xie, J.,
1317 Xue, Y., Masuda, S., Smith, G. C., Balmaseda, M., Germaineaud, C., Lea, D. J., Larnicol, G., Bertino, L.,
1318 Bonaduce, A., ... Usui, N. (2019). Observing System Evaluation Based on Ocean Data Assimilation and
1319 Prediction Systems: On-Going Challenges and a Future Vision for Designing and Supporting Ocean
1320 Observational Networks . In *Frontiers in Marine Science* (Vol. 6, p. 417).
1321 <https://www.frontiersin.org/article/10.3389/fmars.2019.00417>

1322 Gaillard, F., Reynaud, T., Thierry, V., Kolodziejczyk, N., & von Schuckmann, K. (2016). In Situ–Based Reanalysis
1323 of the Global Ocean Temperature and Salinity with ISAS: Variability of the Heat Content and Steric Height.
1324 *Journal of Climate*, 29(4), 1305–1323. <https://doi.org/10.1175/JCLI-D-15-0028.1>

1325 García Molinos, J., Halpern, B. S., Schoeman, D. S., Brown, C. J., Kiessling, W., Moore, P. J., Pandolfi, J. M.,
1326 Poloczanska, E. S., Richardson, A. J., & Burrows, M. T. (2016). Climate velocity and the future global
1327 redistribution of marine biodiversity. *Nature Climate Change*, 6(1), 83–88.
1328 <https://doi.org/10.1038/nclimate2769>

1329 García-García, A., Cuesta-Valero, F. J., Beltrami, H., & Smerdon, J. E. (2016). Simulation of air and ground
1330 temperatures in PMIP3/CMIP5 last millennium simulations: implications for climate reconstructions from
1331 borehole temperature profiles. *Environmental Research Letters*, 11(4), 044022. <https://doi.org/10.1088/1748-9326/11/4/044022>

1333 García-García, Almudena, Cuesta-Valero, F. J., Beltrami, H., & Smerdon, J. E. (2019). Characterization of Air and
1334 Ground Temperature Relationships within the CMIP5 Historical and Future Climate Simulations. *Journal of*
1335 *Geophysical Research: Atmospheres*, 124(7), 3903–3929. <https://doi.org/10.1029/2018JD030117>

1336 Gardner, A. S., Moholdt, G., Cogley, J. G., Wouters, B., Arendt, A. A., Wahr, J., Berthier, E., Hock, R., Pfeffer, W.
1337 T., Kaser, G., Ligtenberg, S. R. M., Bolch, T., Sharp, M. J., Hagen, J. O., van den Broeke, M. R., & Paul, F.
1338 (2013). A Reconciled Estimate of Glacier Contributions to Sea Level Rise: 2003 to 2009. *Science*, 340(6134),
1339 852. <https://doi.org/10.1126/science.1234532>

1340 Gattuso, J.-P., Magnan, A., Billé, R., Cheung, W. W. L., Howes, E. L., Joos, F., Allemand, D., Bopp, L., Cooley, S.
1341 R., Eakin, C. M., Hoegh-Guldberg, O., Kelly, R. P., Pörtner, H.-O., Rogers, A. D., Baxter, J. M., Laffoley, D.,
1342 Osborn, D., Rankovic, A., Rochette, J., ... Turley, C. (2015). Contrasting futures for ocean and society from
1343 different anthropogenic CO₂ emissions scenarios. *Science*, 349(6243), aac4722.
1344 <https://doi.org/10.1126/science.aac4722>

1345 GCOS. (2016). *The Global Observing System for Climate: Implementation needs*.
1346 <https://doi.org/https://doi.org/DOI: 10.13140/RG.2.2.23178.26566>

1347 Gelaro, R., McCarty, W., Suárez, M. J., Todling, R., Molod, A., Takacs, L., Randles, C. A., Darmenov, A.,
1348 Bosilovich, M. G., Reichle, R., Wargan, K., Coy, L., Cullather, R., Draper, C., Akella, S., Buchard, V.,
1349 Conaty, A., da Silva, A. M., Gu, W., ... Zhao, B. (2017). The Modern-Era Retrospective Analysis for
1350 Research and Applications, Version 2 (MERRA-2). *Journal of Climate*, 30(14), 5419–5454.
1351 <https://doi.org/10.1175/JCLI-D-16-0758.1>

1352 Gentine, P., Garcia-Garcia, A., Meier, R., Cuesta-Valero, F., Hugo, B., Davin, E. L., & Seneviratne, S. I. (2020).
1353 Large recent continental heat storage. *Nature, under revi*.

1354 Gleckler, P., Durack, P., Ronald, S., Johnson, G., & Forest, C. (2016). Industrial-era global ocean heat uptake
1355 doubles in recent decades. *Nature Climate Change*, 6. <https://doi.org/10.1038/nclimate2915>

1356 Goni, G. J., Sprintall, J., Bringas, F., Cheng, L., Cirano, M., Dong, S., Domingues, R., Goes, M., Lopez, H.,
1357 Morrow, R., Rivero, U., Rossby, T., Todd, R. E., Trinanés, J., Zilberman, N., Baringer, M., Boyer, T.,
1358 Cowley, R., Domingues, C. M., ... Volkov, D. (2019). More Than 50 Years of Successful Continuous
1359 Temperature Section Measurements by the Global Expendable Bathythermograph Network, Its Integrability,
1360 Societal Benefits, and Future. *Frontiers in Marine Science*, 6, 452.
1361 <https://www.frontiersin.org/article/10.3389/fmars.2019.00452>

1362 González-Rouco, J. F., Beltrami, H., Zorita, E., & Stevens, M. B. (2009). Borehole climatology: a discussion based
1363 on contributions from climate modeling. *Clim. Past*, 5(1), 97–127. <https://doi.org/10.5194/cp-5-97-2009>

1364 González-Rouco, J. F., Beltrami, H., Zorita, E., & von Storch, H. (2006). Simulation and inversion of borehole
1365 temperature profiles in surrogate climates: Spatial distribution and surface coupling. *Geophysical Research*
1366 *Letters*, 33(1). <https://doi.org/10.1029/2005GL024693>

1367 Good, S. A., Martin, M. J., & Rayner, N. A. (2013). EN4: Quality controlled ocean temperature and salinity profiles
1368 and monthly objective analyses with uncertainty estimates. *Journal of Geophysical Research: Oceans*,
1369 118(12), 6704–6716. <https://doi.org/10.1002/2013JC009067>

1370 Gouretski, V., & Cheng, L. (2020). Correction for Systematic Errors in the Global Dataset of Temperature Profiles
1371 from Mechanical Bathythermographs. *Journal of Atmospheric and Oceanic Technology*, 37(5), 841–855.
1372 <https://doi.org/10.1175/JTECH-D-19-0205.1>

1373 Gregory, J. M., & Andrews, T. (2016). Variation in climate sensitivity and feedback parameters during the historical
1374 period. *Geophysical Research Letters*, 43(8), 3911–3920. <https://doi.org/10.1002/2016GL068406>

1375 Gregory, J. M., Andrews, T., Ceppi, P., Mauritsen, T., & Webb, M. J. (2020). How accurately can the climate
1376 sensitivity to CO_2 be estimated from historical climate change? *Climate Dynamics*,
1377 54(1), 129–157. <https://doi.org/10.1007/s00382-019-04991-y>

1378 Guinehut, S., Dhomp, A.-L., Larnicol, G., & Le Traon, P.-Y. (2012). High resolution 3-D temperature and salinity
1379 fields derived from in situ and satellite observations. *Ocean Sci.*, 8(5), 845–857. <https://doi.org/10.5194/os-8-845-2012>

1380 Hansen, J. (2005). Efficacy of climate forcings. *Journal of Geophysical Research*, 110(D18), D18104.
1381 <https://doi.org/10.1029/2005JD005776>

1382 Hansen, J., Sato, M., Kharecha, P., & von Schuckmann, K. (2011). Earth’s energy imbalance and implications.
1383 *Atmos. Chem. Phys.*, 11(24), 13421–13449. <https://doi.org/10.5194/acp-11-13421-2011>

1384 Hansen, J., Sato, M., Kharecha, P., von Schuckmann, K., Beerling, D. J., Cao, J., Marcott, S., Masson-Delmotte, V.,
1385 Prather, M. J., Rohling, E. J., Shakun, J., Smith, P., Lacis, A., Russell, G., & Ruedy, R. (2017). Young
1386 people’s burden: requirement of negative CO₂ emissions. *Earth Syst. Dynam.*, 8(3), 577–616.
1387 <https://doi.org/10.5194/esd-8-577-2017>

1388 Hansen, James, Nazarenko, L., Ruedy, R., Sato, M., Willis, J., Del Genio, A., Koch, D., Lacis, A., Lo, K., Menon,
1389 S., Novakov, T., Perlwitz, J., Russell, G., Schmidt, G. A., & Tausnev, N. (2005). Earth’s Energy
1390 Imbalance: Confirmation and Implications. *Science*, 308(5727), 1431 LP – 1435.
1391 <https://doi.org/10.1126/science.1110252>

1392 Harris, R. N., & Chapman, D. S. (2001). Mid-latitude (30°–60° N) climatic warming inferred by combining
1393 borehole temperatures with surface air temperatures. *Geophysical Research Letters*, 28(5), 747–750.
1394 <https://doi.org/10.1029/2000GL012348>

1395 Hartmann, A., & Rath, V. (2005). Uncertainties and shortcomings of ground surface temperature histories derived
1396 from inversion of temperature logs. *Journal of Geophysics and Engineering*, 2(4), 299–311.
1397 <https://doi.org/10.1088/1742-2132/2/4/S02>

1398 Hermoso de Mendoza, I., Beltrami, H., MacDougall, A. H., & Mareschal, J.-C. (2018). Lower boundary conditions
1399 in Land Surface Models. Effects on the permafrost and the carbon pools. *Geosci. Model Dev. Discuss.*, 2018,
1400 1–34. <https://doi.org/10.5194/gmd-2018-233>

1401 Hersbach, H., Rosnay, P. de, Bell, B., Schepers, D., Simmons, A., Soci, C., Abdalla, S., Alonso-Balmaseda, M.,
1402 Balsamo, G., Bechtold, P., Berrisford, P., Bidlot, J.-R., de Boissés, E., Bonavita, M., Browne, P., Buizza,
1403 R., Dahlgren, P., Dee, D., Dragani, R., ... Zuo, H. (2018). Operational global reanalysis: progress, future
1404 directions and synergies with NWP. In *ERA Report Series* (ERA Report). <https://www.ecmwf.int/node/18765>

1405 Hersbach, H., Bell, B., Berrisford, P., Hirahara, S., Horányi, A., Muñoz-Sabater, J., Nicolas, J., Peubey, C., Radu,
1406 R., Schepers, D., Simmons, A., Soci, C., Abdalla, S., Abellan, X., Balsamo, G., Bechtold, P., Biavati, G.,
1407 Bidlot, J., Bonavita, M., Chiara, G. D., Dahlgren, P., Dee, D., Diamantakis, M., Dragani, R., Flemming, J.,
1408 Forbes, R., Fuentes, M., Geer, A., Haimberger, L., Healy, S., Hogan, R. J., Hólm, E., Janisková, M., Keeley,
1409 S., Laloyaux, P., Lopez, P., Lupu, C., Radnoti, G., Rosnay, P. de, Rozum, I., Vamborg, F., Villaume, S. &
1410 Thépaut, J.-N. (2020). The ERA5 global reanalysis. *Q. J. R. Meteorol. Soc.* <https://doi.org/10.1002/qj.3803>.

1411 Hicks Pries, C. E., Castanha, C., Porras, R., & Torn, M. S. (2017). The whole-soil carbon flux in response to
1412 warming. *Science*, eaal1319. <https://doi.org/10.1126/science.aal1319>

1413 Hoegh-Guldberg, O., et al. (2018). *Global Warming on Natural and Human Systems*. In: *Global Warming of 1.5°C*.
1414 *An IPCC Special Report on the impacts of global warming of 1.5°C above pre-industrial levels and related*
1415 *global greenhouse gas emission pathways, in the context of strengthening the*

1416 Hopcroft, P. O., Gallagher, K., & Pain, C. C. (2007). Inference of past climate from borehole temperature data using

1418 Bayesian Reversible Jump Markov chain Monte Carlo. *Geophysical Journal International*, 171(3), 1430–
1419 1439. <https://doi.org/10.1111/j.1365-246X.2007.03596.x>

1420 Huang, S. (2006). 1851–2004 annual heat budget of the continental landmasses. *Geophysical Research Letters*,
1421 33(4). <https://doi.org/10.1029/2005GL025300>

1422 Huang, S., Pollack, H. N., & Shen, P.-Y. (2000). Temperature trends over the past five centuries reconstructed from
1423 borehole temperatures. *Nature*, 403(6771), 756–758. <https://doi.org/10.1038/35001556>

1424 IPCC Special Report on the Ocean and Cryosphere in a Changing Climate. (2019). In H. O. Pörtner, D. C. Roberts,
1425 V. Masson-Delmotte, P. Zhai, M. Tignor, E. Poloczanska, K. Mintenbeck, A. Alegria, M. Nicolai, A. Okem, J.
1426 Petzold, B. Rama, & N. M. Weyer (Eds.), *IPCC Intergovernmental Panel on Climate Change: Geneva*,
1427 Switzerland. <https://www.ipcc.ch/srocc/>

1428 Ishii, M., Fukuda, Y., Hirahara, S., Yasui, S., Suzuki, T., & Sato, K. (2017). Accuracy of Global Upper Ocean Heat
1429 Content Estimation Expected from Present Observational Data Sets. *SOLA*, 13, 163–167.
1430 <https://doi.org/10.2151/sola.2017-030>

1431 Jacobs, S. S., Giulivi, C. F., & Mele, P. A. (2002). Freshening of the Ross Sea During the Late 20th Century.
1432 *Science*, 297(5580), 386. <https://doi.org/10.1126/science.1069574>

1433 Jaume-Santero, F., Pickler, C., Beltrami, H., & Mareschal, J.-C. (2016). North American regional climate
1434 reconstruction from ground surface temperature histories. *Clim. Past*, 12(12), 2181–2194.
1435 <https://doi.org/10.5194/cp-12-2181-2016>

1436 Jeong, D. Il, Sushama, L., Diro, G. T., Khaliq, M. N., Beltrami, H., & Caya, D. (2016). Projected changes to high
1437 temperature events for Canada based on a regional climate model ensemble. *Climate Dynamics*, 46(9), 3163–
1438 3180. <https://doi.org/10.1007/s00382-015-2759-y>

1439 Johnson, G.C., Lyman, J.M., Boyer, T., Cheng, L., Domingues, C.M., Gilson, J., Ishii, M., Killick, R., Monselesan,
1440 D., Purkey, S.G., Wijffels, S. E. (2018). Ocean heat content [in State of the Climate in 2017]. *Bulletin of the*
1441 *American Meteorological Society*, 99(8), S72–S77.

1442 Johnson, G. C., & Birnbaum, A. N. (2017). As El Niño builds, Pacific Warm Pool expands, ocean gains more heat.
1443 *Geophysical Research Letters*, 44(1), 438–445. <https://doi.org/10.1002/2016GL071767>

1444 Johnson, G. C., Lyman, J. M., & Purkey, S. G. (2015). Informing Deep Argo Array Design Using Argo and Full-
1445 Depth Hydrographic Section Data*. *Journal of Atmospheric and Oceanic Technology*, 32(11), 2187–2198.
1446 <https://doi.org/10.1175/JTECH-D-15-0139.1>

1447 Johnson, G. C., Purkey, S. G., Zilberman, N. V., & Roemmich, D. (2019). Deep Argo Quantifies Bottom Water
1448 Warming Rates in the Southwest Pacific Basin. *Geophysical Research Letters*, 46(5), 2662–2669.
1449 <https://doi.org/10.1029/2018GL081685>

1450 King, B. A., Firing, E., & M.Joyce, T. (2001). Chapter 3.1 Shipboard observations during WOCE. *International*
1451 *Geophysics*, 77, 99–122. [https://doi.org/10.1016/S0074-6142\(01\)80114-5](https://doi.org/10.1016/S0074-6142(01)80114-5)

1452 King, M. D., Howat, I. M., Jeong, S., Noh, M. J., Wouters, B., Noël, B., & van den Broeke, M. R. (2018). Seasonal
1453 to decadal variability in ice discharge from the Greenland Ice Sheet. *The Cryosphere*, 12(12), 3813–3825.
1454 <https://doi.org/10.5194/tc-12-3813-2018>

1455 King, M.D., Howat, I.M., Candela, S.G. et al. Dynamic ice loss from the Greenland Ice Sheet driven by sustained
1456 glacier retreat. *Commun Earth Environ* 1, 1 (2020). <https://doi.org/10.1038/s43247-020-0001-2>

1457 Kirchengast, G., Ladstädter, F., Steiner, A. K., Gorfer, M., Lippl, F., & Angerer, B. (2019). *Climate trends and*
1458 *variability in atmosphere heat content and atmosphere-ocean heat exchanges: space geodesy is key*. (No.
1459 IUGG19-4651). [https://www.czech-](https://www.czech-in.org/cmPortalV15/CM_W3_Searchable/iugg19/normal#!sessiondetails/0000119801_0)
1460 [in.org/cmPortalV15/CM_W3_Searchable/iugg19/normal#!sessiondetails/0000119801_0](https://www.czech-in.org/cmPortalV15/CM_W3_Searchable/iugg19/normal#!sessiondetails/0000119801_0)

1461 Knutti, R., & Rugenstein, M. A. A. (2015). Feedbacks, climate sensitivity and the limits of linear models.
1462 *Philosophical Transactions of the Royal Society A: Mathematical, Physical and Engineering Sciences*,
1463 373(2054), 20150146. <https://doi.org/10.1098/rsta.2015.0146>

1464 Kobayashi, S., Ota, Y., Harada, Y., Ebata, A., Moriya, M., Onoda, H., Onogi, K., Kamahori, H., Kobayashi, C.,
1465 Endo, H., Miyaoka, K., & Takahashi, K. (2015). The JRA-55 Reanalysis: General Specifications and Basic
1466 Characteristics. *Journal of the Meteorological Society of Japan. Ser. II*, 93(1), 5–48.
1467 <https://doi.org/10.2151/jmsj.2015-001>

1468 Kuhlbrodt, T., & Gregory, J. M. (2012). Ocean heat uptake and its consequences for the magnitude of sea level rise
1469 and climate change. *Geophysical Research Letters*, 39(18). <https://doi.org/10.1029/2012GL052952>

1470 Labe, Z., Magnusdottir, G., & Stern, H. (2018). Variability of Arctic Sea Ice Thickness Using PIOMAS and the
1471 CESM Large Ensemble. *Journal of Climate*, 31(8), 3233–3247. <https://doi.org/10.1175/JCLI-D-17-0436.1>

1472 Lachenbruch, A. H., & Marshall, B. V. (1986). Changing Climate: Geothermal Evidence from Permafrost in the
1473 Alaskan Arctic. *Science*, 234(4777), 689–696. www.jstor.org/stable/1697932

- 1474 Ladstädter, F., Steiner, A. K., Schwärz, M., & Kirchengast, G. (2015). Climate intercomparison of GPS radio
1475 occultation, RS90/92 radiosondes and GRUAN from 2002 to 2013. *Atmos. Meas. Tech.*, 8(4), 1819–1834.
1476 <https://doi.org/10.5194/amt-8-1819-2015>
- 1477 Lane, A. C. (1923). Geotherms of Lake Superior Copper Country. *GSA Bulletin*, 34(4), 703–720.
1478 <https://doi.org/10.1130/GSAB-34-703>
- 1479 Laxon, S. W., Giles, K. A., Ridout, A. L., Wingham, D. J., Willatt, R., Cullen, R., Kwok, R., Schweiger, A., Zhang,
1480 J., Haas, C., Hendricks, S., Krishfield, R., Kurtz, N., Farrell, S., & Davidson, M. (2013). CryoSat-2 estimates
1481 of Arctic sea ice thickness and volume. *Geophysical Research Letters*, 40(4), 732–737.
1482 <https://doi.org/10.1002/grl.50193>
- 1483 Leifeld, J., Wüst-Galley, C., & Page, S. (2019). Intact and managed peatland soils as a source and sink of GHGs
1484 from 1850 to 2100. *Nature Climate Change*, 9(12), 945–947. <https://doi.org/10.1038/s41558-019-0615-5>
- 1485 Lembo, V., Folini, D., Wild, M., & Lionello, P. (2019). Inter-hemispheric differences in energy budgets and cross-
1486 equatorial transport anomalies during the 20th century. *Climate Dynamics*, 53(1), 115–135.
1487 <https://doi.org/10.1007/s00382-018-4572-x>
- 1488 Lenton, T. M. (2011). Early warning of climate tipping points. *Nature Climate Change*, 1(4), 201–209.
1489 <https://doi.org/10.1038/nclimate1143>
- 1490 Lenton, T. M., Held, H., Kriegler, E., Hall, J. W., Lucht, W., Rahmstorf, S., & Schellnhuber, H. J. (2008). Tipping
1491 elements in the Earth’s climate system. *Proceedings of the National Academy of Sciences of the United States*
1492 *of America*, 105(6), 1786–1793. <https://doi.org/10.1073/pnas.0705414105>
- 1493 Lenton, T., Rockström, J., Gaffney, O., Rahmstorf, S., Richardson, K., Steffen, W., & Schellnhuber, H. (2019).
1494 Climate tipping points — too risky to bet against. *Nature*, 575, 592–595. <https://doi.org/10.1038/d41586-019-03595-0>
- 1496 Levitus, S., Antonov, J. I., Boyer, T. P., Baranova, O. K., Garcia, H. E., Locarnini, R. A., Mishonov, A. V., Reagan,
1497 J. R., Seidov, D., Yarosh, E. S., & Zweng, M. M. (2012). World ocean heat content and thermocline sea level
1498 change (0–2000 m), 1955–2010. *Geophysical Research Letters*, 39(10).
1499 <https://doi.org/10.1029/2012GL051106>
- 1500 Ligtenberg, S. R. M., Kuipers Munneke, P., Noël, B. P. Y., & van den Broeke, M. R. (2018). Brief communication:
1501 Improved simulation of the present-day Greenland firn layer (1960–2016). *The Cryosphere*, 12(5), 1643–
1502 1649. <https://doi.org/10.5194/tc-12-1643-2018>
- 1503 Llovel, W., Willis, J. K., Landerer, F. W., & Fukumori, I. (2014). Deep-ocean contribution to sea level and energy
1504 budget not detectable over the past decade. *Nature Climate Change*, 4(11), 1031–1035.
1505 <https://doi.org/10.1038/nclimate2387>
- 1506 Loeb, N. G., Lyman, J. M., Johnson, G. C., Allan, R. P., Doelling, D. R., Wong, T., Soden, B. J., & Stephens, G. L.
1507 (2012). Observed changes in top-of-the-atmosphere radiation and upper-ocean heating consistent within
1508 uncertainty. *Nature Geoscience*, 5(2), 110–113. <https://doi.org/10.1038/ngeo1375>
- 1509 Lyman, J. M., & Johnson, G. C. (2013). Estimating Global Ocean Heat Content Changes in the Upper 1800 m since
1510 1950 and the Influence of Climatology Choice. *Journal of Climate*, 27(5), 1945–1957.
1511 <https://doi.org/10.1175/JCLI-D-12-00752.1>
- 1512 MacDougall, A. H., Avis, C. A., & Weaver, A. J. (2012). Significant contribution to climate warming from the
1513 permafrost carbon feedback. *Nature Geoscience*, 5(10), 719–721. <https://doi.org/10.1038/ngeo1573>
- 1514 MacDougall, A. H., Beltrami, H., González-Rouco, J. F., Stevens, M. B., & Bourlon, E. (2010). Comparison of
1515 observed and general circulation model derived continental subsurface heat flux in the Northern Hemisphere.
1516 *Journal of Geophysical Research: Atmospheres*, 115(D12). <https://doi.org/10.1029/2009JD013170>
- 1517 MacDougall, A. H., González-Rouco, J. F., Stevens, M. B., & Beltrami, H. (2008). Quantification of subsurface heat
1518 storage in a GCM simulation. *Geophysical Research Letters*, 35(13). <https://doi.org/10.1029/2008GL034639>
- 1519 Mankoff, K. D., Colgan, W., Solgaard, A., Karlsson, N. B., Ahlstrøm, A. P., van As, D., Box, J. E., Khan, S. A.,
1520 Kjeldsen, K. K., Mougnot, J., & Fausto, R. S. (2019). Greenland Ice Sheet solid ice discharge from 1986
1521 through 2017. *Earth Syst. Sci. Data*, 11(2), 769–786. <https://doi.org/10.5194/essd-11-769-2019>
- 1522 Marshall, J., Scott, J. R., Armour, K. C., Campin, J.-M., Kelley, M., & Romanou, A. (2015). The ocean’s role in the
1523 transient response of climate to abrupt greenhouse gas forcing. *Climate Dynamics*, 44(7), 2287–2299.
1524 <https://doi.org/10.1007/s00382-014-2308-0>
- 1525 Marvel, K., Pincus, R., Schmidt, G. A., & Miller, R. L. (2018). Internal Variability and Disequilibrium Confound
1526 Estimates of Climate Sensitivity From Observations. *Geophysical Research Letters*, 45(3), 1595–1601.
1527 <https://doi.org/10.1002/2017GL076468>
- 1528 Marzeion, B., Leclercq, P. W., Cogley, J. G., & Jarosch, A. H. (2015). Brief Communication: Global reconstructions
1529 of glacier mass change during the 20th century are consistent. *The Cryosphere*, 9(6), 2399–2404.

1530 <https://doi.org/10.5194/tc-9-2399-2015>

1531 Matthews, T. K. R., Wilby, R. L., & Murphy, C. (2017). Communicating the deadly consequences of global
1532 warming for human heat stress. *Proceedings of the National Academy of Sciences*, *114*(15), 3861.
1533 <https://doi.org/10.1073/pnas.1617526114>

1534 Mayer, M., Fasullo, J. T., Trenberth, K. E., & Haimberger, L. (2016). ENSO-driven energy budget perturbations in
1535 observations and CMIP models. *Climate Dynamics*, *47*(12), 4009–4029. <https://doi.org/10.1007/s00382-016-3057-z>

1536

1537 Mayer, M., Haimberger, L., & Balmaseda, M. A. (2014). On the Energy Exchange between Tropical Ocean Basins
1538 Related to ENSO*. *Journal of Climate*, *27*(17), 6393–6403. <https://doi.org/10.1175/JCLI-D-14-00123.1>

1539 Mayer, M., Haimberger, L., Edwards, J. M., & Hyder, P. (2017). Toward Consistent Diagnostics of the Coupled
1540 Atmosphere and Ocean Energy Budgets. *Journal of Climate*, *30*(22), 9225–9246.
1541 <https://doi.org/10.1175/JCLI-D-17-0137.1>

1542 Mayer, M., Tietsche, S., Haimberger, L., Tsubouchi, T., Mayer, J., & Zuo, H. (2019). An Improved Estimate of the
1543 Coupled Arctic Energy Budget. *Journal of Climate*, *32*(22), 7915–7934. <https://doi.org/10.1175/JCLI-D-19-0233.1>

1544

1545 Mayer, M., Trenberth, K. E., Haimberger, L., & Fasullo, J. T. (2013). The Response of Tropical Atmospheric
1546 Energy Budgets to ENSO*. *Journal of Climate*, *26*(13), 4710–4724. <https://doi.org/10.1175/JCLI-D-12-00681.1>

1547

1548 McPherson, M., García-García, A., Cuesta-Valero Francisco, J., Beltrami, H., Hansen-Ketchum, P., MacDougall,
1549 D., & Ogden Nicholas, H. (2017). Expansion of the Lyme Disease Vector *Ixodes Scapularis* in Canada
1550 Inferred from CMIP5 Climate Projections. *Environmental Health Perspectives*, *125*(5), 057008.
1551 <https://doi.org/10.1289/EHP57>

1552 Mears, C. A., & Wentz, F. J. (2009a). Construction of the Remote Sensing Systems V3.2 Atmospheric Temperature
1553 Records from the MSU and AMSU Microwave Sounders. *Journal of Atmospheric and Oceanic Technology*,
1554 *26*(6), 1040–1056. <https://doi.org/10.1175/2008JTECHA1176.1>

1555 Mears, C. A., & Wentz, F. J. (2009b). Construction of the RSS V3.2 Lower-Tropospheric Temperature Dataset from
1556 the MSU and AMSU Microwave Sounders. *Journal of Atmospheric and Oceanic Technology*, *26*(8), 1493–
1557 1509. <https://doi.org/10.1175/2009JTECHA1237.1>

1558 Mears, C. A., & Wentz, F. J. (2017). A Satellite-Derived Lower-Tropospheric Atmospheric Temperature Dataset
1559 Using an Optimized Adjustment for Diurnal Effects. *Journal of Climate*, *30*(19), 7695–7718.
1560 <https://doi.org/10.1175/JCLI-D-16-0768.1>

1561 Melo-Aguilar, C., González-Rouco, J. F., García-Bustamante, E., Navarro-Montesinos, J., & Steinert, N. (2018).
1562 Influence of radiative forcing factors on ground–air temperature coupling during the last millennium:
1563 implications for borehole climatology. *Clim. Past*, *14*(11), 1583–1606. <https://doi.org/10.5194/cp-14-1583-2018>

1564

1565 Meyssignac, B., Boyer, T., Zhao, Z., Hakuba, M. Z., Landerer, F. W., Stammer, D., Köhl, A., Kato, S., L’Ecuyer,
1566 T., Ablain, M., Abraham, J. P., Blazquez, A., Cazenave, A., Church, J. A., Cowley, R., Cheng, L., Domingues,
1567 C. M., Giglio, D., Gouretski, V., ... Zilberman, N. (2019). Measuring Global Ocean Heat Content to Estimate
1568 the Earth Energy Imbalance. *Frontiers in Marine Science*, *6*, 432.
1569 <https://www.frontiersin.org/article/10.3389/fmars.2019.00432>

1570 Mouginit, J., Rignot, E., Björk, A. A., van den Broeke, M., Millan, R., Morlighem, M., Noël, B., Scheuchl, B., &
1571 Wood, M. (2019). Forty-six years of Greenland Ice Sheet mass balance from 1972 to 2018. *Proceedings of the*
1572 *National Academy of Sciences*, *116*(19), 9239. <https://doi.org/10.1073/pnas.1904242116>

1573 Myhre, G., Shindell, D., Bréon, F.-M., Collins, W., Fuglestedt, J., Huang, J., Koch, D., Lamarque, J.-F., Lee, D.,
1574 Mendoza, B., Nakajima, T., Robock, A., Stephens, G., Takemura, T., & Zhang, H. (2013). Anthropogenic and
1575 natural radiative forcing. In *Climate Change 2013 the Physical Science Basis: Working Group I Contribution*
1576 *to the Fifth Assessment Report of the Intergovernmental Panel on Climate Change* (Vol. 9781107057, pp.
1577 659–740). <https://doi.org/10.1017/CBO9781107415324.018>

1578 Nauels, A., Meinshausen, M., Mengel, M., Lorbacher, K., & Wigley, T. M. L. (2017). Synthesizing long-term sea
1579 level rise projections – the MAGICC sea level model v2.0. *Geosci. Model Dev.*, *10*(6), 2495–2524.
1580 <https://doi.org/10.5194/gmd-10-2495-2017>

1581 Noël, B., van de Berg, W. J., van Wessem, J. M., van Meijgaard, E., van As, D., Lenaerts, J. T. M., Lhermitte, S.,
1582 Kuipers Munneke, P., Smeets, C. J. P. P., van Uft, L. H., van de Wal, R. S. W., & van den Broeke, M. R.
1583 (2018). Modelling the climate and surface mass balance of polar ice sheets using RACMO2 – Part 1:
1584 Greenland (1958–2016). *The Cryosphere*, *12*(3), 811–831. <https://doi.org/10.5194/tc-12-811-2018>

1585 Palmer, M D, & McNeall, D. J. (2014). Internal variability of Earth’s energy budget simulated by CMIP5 climate

1586 models. *Environmental Research Letters*, 9(3), 034016. <https://doi.org/10.1088/1748-9326/9/3/034016>

1587 Palmer, M D, Roberts, C. D., Balmaseda, M., Chang, Y.-S., Chepurin, G., Ferry, N., Fujii, Y., Good, S. A.,

1588 Guinehut, S., Haines, K., Hernandez, F., Köhl, A., Lee, T., Martin, M. J., Masina, S., Masuda, S., Peterson, K.

1589 A., Storto, A., Toyoda, T., ... Xue, Y. (2017). Ocean heat content variability and change in an ensemble of

1590 ocean reanalyses. *Climate Dynamics*, 49(3), 909–930. <https://doi.org/10.1007/s00382-015-2801-0>

1591 Palmer, Matthew D, Durack, P. J., Chidichimo, M. P., Church, J. A., Cravatte, S., Hill, K., Johannessen, J. A.,

1592 Karstensen, J., Lee, T., Legler, D., Mazloff, M., Oka, E., Purkey, S., Rabe, B., Sallée, J.-B., Sloyan, B. M.,

1593 Speich, S., von Schuckmann, K., Willis, J., & Wijffels, S. (2019). Adequacy of the Ocean Observation System

1594 for Quantifying Regional Heat and Freshwater Storage and Change . In *Frontiers in Marine Science* (Vol.

1595 6, p. 416). <https://www.frontiersin.org/article/10.3389/fmars.2019.00416>

1596 Palmer, Matthew D, Harris, G. R., & Gregory, J. M. (2018). Extending CMIP5 projections of global mean

1597 temperature change and sea level rise due to thermal expansion using a physically-based emulator.

1598 *Environmental Research Letters*, 13(8), 084003. <https://doi.org/10.1088/1748-9326/aad2e4>

1599 Parkes, D., & Marzeion, B. (2018). Twentieth-century contribution to sea-level rise from uncharted glaciers. *Nature*,

1600 563(7732), 551–554. <https://doi.org/10.1038/s41586-018-0687-9>

1601 Parkinson, C. L. (2019). A 40-y record reveals gradual Antarctic sea ice increases followed by decreases at rates far

1602 exceeding the rates seen in the Arctic. *Proceedings of the National Academy of Sciences*, 116(29), 14414.

1603 <https://doi.org/10.1073/pnas.1906556116>

1604 Peixoto, J. P., & Oort, A. H. (1992). *Physics of climate*. New York, NY (United States); American Institute of

1605 Physics. <https://www.osti.gov/servlets/purl/7287064>

1606 Pickler, C., Fausto, E., Beltrami, H., Mareschal, jean-claude, Suárez, F., Chacon-Oecklers, A., Blin, N., Calderón,

1607 M., Montenegro, A., Harris, R., & Tassara, A. (2018). Recent climate variations in Chile: Constraints from

1608 borehole temperature profiles. *Climate of the Past*, 14, 559–575. <https://doi.org/10.5194/cp-14-559-2018>

1609 Pollack, H. N., & Smerdon, J. E. (2004). Borehole climate reconstructions: Spatial structure and hemispheric

1610 averages. *Journal of Geophysical Research: Atmospheres*, 109(D11). <https://doi.org/10.1029/2003JD004163>

1611 Polyakov, I. V, Pnyushkov, A. V, Alkire, M. B., Ashik, I. M., Baumann, T. M., Carmack, E. C., Goszczko, I.,

1612 Guthrie, J., Ivanov, V. V, Kanzow, T., Krishfield, R., Kwok, R., Sundfjord, A., Morison, J., Rember, R., &

1613 Yulin, A. (2017). Greater role for Atlantic inflows on sea-ice loss in the Eurasian Basin of the Arctic Ocean.

1614 *Science*, 356(6335), 285. <https://doi.org/10.1126/science.aai8204>

1615 Pritchard, H. D., Ligtenberg, S. R. M., Fricker, H. A., Vaughan, D. G., van den Broeke, M. R., & Padman, L.

1616 (2012). Antarctic ice-sheet loss driven by basal melting of ice shelves. *Nature*, 484(7395), 502–505.

1617 <https://doi.org/10.1038/nature10968>

1618 Purkey, S. G., & Johnson, G. C. (2010). Warming of Global Abyssal and Deep Southern Ocean Waters between the

1619 1990s and 2000s: Contributions to Global Heat and Sea Level Rise Budgets. *Journal of Climate*, 23(23),

1620 6336–6351. <https://doi.org/10.1175/2010JCLI3682.1>

1621 Ramírez, F., Afán, I., Davis, L. S., & Chiaradia, A. (2017). Climate impacts on global hot spots of marine

1622 biodiversity. *Science Advances*, 3(2), e1601198. <https://doi.org/10.1126/sciadv.1601198>

1623 Rhein, M., Rintoul, S., Aoki, S., Campos, E., Chambers, D., Feely, R., Gulev, S., Johnson, G., Josey, S., Kostianoy,

1624 A., Mauritzen, C., Roemmich, D., Talley, L., & Wang, F. (2013). *Observations: Ocean. In: Climate Change*

1625 *2013: The Physical Science Basis. Contribution of Working Group I to the Fifth Assessment Report of the*

1626 *Intergovernmental Panel on Climate Change*].

1627 Rhein, M, Rintoul, S., Aoki, S., Campos, E., Change, D. C.-C., & 2013, undefined. (n.d.). *Observations: ocean*

1628 *(Contribution of Working Group I to the Fifth Assessment Report of the Intergovernmental Panel on Climate*

1629 *Change)*.

1630 Rhein, Monika, Steinfeldt, R., Huhn, O., Sültenfuß, J., & Breckenfelder, T. (2018). Greenland Submarine Melt

1631 Water Observed in the Labrador and Irminger Sea. *Geophysical Research Letters*, 45(19), 10, 510–570, 578.

1632 <https://doi.org/10.1029/2018GL079110>

1633 Richter-Menge, J., M.L. Druckenmiller, and M. Jeffries, Eds., 2019: Arctic Report Card, 2019.

1634 <https://www.arctic.noaa.gov/Report-Card>.

1635 Rignot, E., Mouginot, J., Scheuchl, B., van den Broeke, M., van Wessem, M. J., & Morlighem, M. (2019). Four

1636 decades of Antarctic Ice Sheet mass balance from 1979–2017. *Proceedings of the National Academy of*

1637 *Sciences*, 116(4), 1095. <https://doi.org/10.1073/pnas.1812883116>

1638 Riser, S. C., Freeland, H. J., Roemmich, D., Wijffels, S., Troisi, A., Belbéoch, M., Gilbert, D., Xu, J., Pouliquen, S.,

1639 Thresher, A., Le Traon, P.-Y., Maze, G., Klein, B., Ravichandran, M., Grant, F., Poulain, P.-M., Suga, T.,

1640 Lim, B., Sterl, A., ... Jayne, S. R. (2016). Fifteen years of ocean observations with the global Argo array.

1641 *Nature Climate Change*, 6(2), 145–153. <https://doi.org/10.1038/nclimate2872>

- 1642 Roemmich, D., & Gilson, J. (2009). The 2004–2008 mean and annual cycle of temperature, salinity, and steric
1643 height in the global ocean from the Argo Program. *Progress in Oceanography*, 82(2), 81–100.
1644 <https://doi.org/https://doi.org/10.1016/j.pocean.2009.03.004>
- 1645 Roy, S., Harris, R. N., Rao, R. U. M., & Chapman, D. S. (2002). Climate change in India inferred from geothermal
1646 observations. *Journal of Geophysical Research: Solid Earth*, 107(B7), ETG 5-1-ETG 5-16.
1647 <https://doi.org/10.1029/2001JB000536>
- 1648 Santer, B. D., Po-Chedley, S., Zelinka, M. D., Cvijanovic, I., Bonfils, C., Durack, P. J., Fu, Q., Kiehl, J., Mears, C.,
1649 Painter, J., Pallotta, G., Solomon, S., Wentz, F. J., & Zou, C.-Z. (2018). Human influence on the seasonal
1650 cycle of tropospheric temperature. *Science*, 361(6399), eaas8806. <https://doi.org/10.1126/science.aas8806>
- 1651 Santer, B. D., Solomon, S., Wentz, F. J., Fu, Q., Po-Chedley, S., Mears, C., Painter, J. F., & Bonfils, C. (2017).
1652 Tropospheric Warming Over The Past Two Decades. *Scientific Reports*, 7(1), 2336.
1653 <https://doi.org/10.1038/s41598-017-02520-7>
- 1654 Schweiger, A. J., Wood, K. R., & Zhang, J. (2019). Arctic Sea Ice Volume Variability over 1901–2010: A Model-
1655 Based Reconstruction. *Journal of Climate*, 32(15), 4731–4752. <https://doi.org/10.1175/JCLI-D-19-0008.1>
- 1656 Schweiger, A., Lindsay, R., Zhang, J., Steele, M., Stern, H., & Kwok, R. (2011). Uncertainty in modeled Arctic sea
1657 ice volume. *Journal of Geophysical Research: Oceans*, 116(C8). <https://doi.org/10.1029/2011JC007084>
- 1658 Seneviratne, S., Donat, M., Mueller, B., & Alexander, L. (2014). No pause in the increase of hot temperature
1659 extremes. *Nature Climate Change*, 4. <https://doi.org/10.1038/nclimate2145>
- 1660 Seneviratne, S. I., Corti, T., Davin, E. L., Hirschi, M., Jaeger, E. B., Lehner, I., Orlowsky, B., & Teuling, A. J.
1661 (2010). Investigating soil moisture–climate interactions in a changing climate: A review. *Earth-Science
1662 Reviews*, 99(3–4), 125–161. <https://doi.org/10.1016/J.EARSCIREV.2010.02.004>
- 1663 Seneviratne, S., Lüthi, D., Litschi, M., & Schär, C. (2006). Land-atmosphere coupling and climate change in
1664 Europe. *Nature*, 443, 205–209. <https://doi.org/10.1038/nature05095>
- 1665 Serreze, M. C., & Barry, R. G. (2011). Processes and impacts of Arctic amplification: A research synthesis. *Global
1666 and Planetary Change*, 77(1–2), 85–96. <https://doi.org/10.1016/J.GLOPLACHA.2011.03.004>
- 1667 Shepherd, A., Fricker, H. A., & Farrell, S. L. (2018). Trends and connections across the Antarctic cryosphere.
1668 *Nature*, 558(7709), 223–232. <https://doi.org/10.1038/s41586-018-0171-6>
- 1669 Shepherd, A., Ivins, E., Rignot, E., Smith, B., van den Broeke, M., Velicogna, I., Whitehouse, P., Briggs, K.,
1670 Joughin, I., Krinner, G., Nowicki, S., Payne, T., Scambos, T., Schlegel, N., A, G., Agosta, C., Ahlstrøm, A.,
1671 Babonis, G., Barletta, V., ... team, T. I. (2018). Mass balance of the Antarctic Ice Sheet from 1992 to 2017.
1672 *Nature*, 558(7709), 219–222. <https://doi.org/10.1038/s41586-018-0179-y>
- 1673 Sherwood, S. C., & Huber, M. (2010). An adaptability limit to climate change due to heat stress. *Proceedings of the
1674 National Academy of Sciences*, 107(21), 9552. <https://doi.org/10.1073/pnas.0913352107>
- 1675 Shi, J.-R., Xie, S.-P., & Talley, L. D. (2018). Evolving Relative Importance of the Southern Ocean and North
1676 Atlantic in Anthropogenic Ocean Heat Uptake. *Journal of Climate*, 31(18), 7459–7479.
1677 <https://doi.org/10.1175/JCLI-D-18-0170.1>
- 1678 Smerdon, J. E., & Stieglitz, M. (2006). Simulating heat transport of harmonic temperature signals in the Earth’s
1679 shallow subsurface: Lower-boundary sensitivities. *Geophysical Research Letters*, 33(14).
1680 <https://doi.org/10.1029/2006GL026816>
- 1681 Steiner, A., Ladstädter, F., Randel, W. J., Maycock, A. C., Claud, C., Fu, Q., Gleisner, H., Haimberger, L., Ho, S.-
1682 P., Keckhut, P., Leblanc, T., Mears, C., Polvani, L., Santer, B., Schmidt, T., Sofieva, V., Wing, R., & Zou, C.-
1683 Z. (2020). Observed temperature changes in the troposphere and stratosphere from 1979 to 2018. *Journal of
1684 Climate*, <https://doi.org/doi:10.1175/JCLI-D-19-0998.1>
- 1685 Stevens, C. W. (2007). *Subsurface investigation of shallow-water permafrost located within the near-shore zone of
1686 the Mackenzie Delta, Northwest Territories, Canada*. University of Calgary.
- 1687 Stevens, M. B., González-Rouco, J. F., & Beltrami, H. (2008). North American climate of the last millennium:
1688 Underground temperatures and model comparison. *Journal of Geophysical Research: Earth Surface*, 113(F1).
1689 <https://doi.org/10.1029/2006JF000705>
- 1690 Stieglitz, M., & Smerdon, J. E. (2007). Characterizing Land–Atmosphere Coupling and the Implications for
1691 Subsurface Thermodynamics. *Journal of Climate*, 20(1), 21–37. <https://doi.org/10.1175/JCLI3982.1>
- 1692 Storto, A., Alvera-Azcárate, A., Balmaseda, M. A., Barth, A., Chevallier, M., Counillon, F., Domingues, C. M.,
1693 Drevillon, M., Drillet, Y., Forget, G., Garric, G., Haines, K., Hernandez, F., Iovino, D., Jackson, L. C.,
1694 Lellouche, J.-M., Masina, S., Mayer, M., Oke, P. R., ... Zuo, H. (2019). Ocean Reanalyses: Recent Advances
1695 and Unsolved Challenges. *Frontiers in Marine Science*, 6, 418. <https://doi.org/10.3389/fmars.2019.00418>
- 1696 Storto, A., Masina, S., Simoncelli, S., Iovino, D., Cipollone, A., Drevillon, M., Drillet, Y., Schuckman, K., Parent,
1697 L., Garric, G., Greiner, E., Desportes, C., Zuo, H., Balmaseda, M., & Peterson, K. (2018). The added value of

1698 the multi-system spread information for ocean heat content and steric sea level investigations in the CMEMS
1699 GREP ensemble reanalysis product. *Climate Dynamics*. <https://doi.org/10.1007/s00382-018-4585-5>

1700 Straneo, F., Adusumilli, S., Slater, D., Timmermanns, M., Marzeion, B., & Schweiger, A. (2020). Inventory of
1701 Earth's ice loss and associated energy uptake from 1979 to 2017. *Geophysical Research Letters*,
1702 *submitted*.

1703 Straneo, Fiamma, & Cenedese, C. (2015). The Dynamics of Greenland's Glacial Fjords and Their Role in Climate.
1704 *Annual Review of Marine Science*, 7(1), 89–112. <https://doi.org/10.1146/annurev-marine-010213-135133>

1705 Suman, A., Dyer, F., & White, D. (2017). Late Holocene temperature variability in Tasmania inferred from borehole
1706 temperature data. *Clim. Past*, 13(6), 559–572. <https://doi.org/10.5194/cp-13-559-2017>

1707 Trenberth, K. E., Cheng, L., Jacobs, P., Zhang, Y., & Fasullo, J. (2018). Hurricane Harvey Links to Ocean Heat
1708 Content and Climate Change Adaptation. *Earth's Future*, 6(5), 730–744.
1709 <https://doi.org/10.1029/2018EF000825>

1710 Trenberth, K. E., & Fasullo, J. T. (2010). Tracking Earth's Energy. *Science*, 328(5976), 316.
1711 <https://doi.org/10.1126/science.1187272>

1712 Trenberth, K. E., & Fasullo, J. T. (2018). Applications of an Updated Atmospheric Energetics Formulation. *Journal*
1713 *of Climate*, 31(16), 6263–6279. <https://doi.org/10.1175/JCLI-D-17-0838.1>

1714 Trenberth, K. E., Fasullo, J. T., & Shepherd, T. G. (2015). Attribution of climate extreme events. *Nature Climate*
1715 *Change*, 5(8), 725–730. <https://doi.org/10.1038/nclimate2657>

1716 Trenberth, K. E., Fasullo, J. T., von Schuckmann, K., & Cheng, L. (2016). Insights into Earth's Energy Imbalance
1717 from Multiple Sources. *Journal of Climate*, 29(20), 7495–7505. <https://doi.org/10.1175/JCLI-D-16-0339.1>

1718 UN. (1992). *United Nations Framework Convention on Climate Change, FCCC/INFORMAL/84 GE.05-62220 (E)*
1719 *200705*. <https://unfccc.int/resource/docs/convkp/conveng.pdf>

1720 UN. (2015). *The Paris Agreement*. https://unfccc.int/sites/default/files/english_paris_agreement.pdf

1721 UNGA. (2012). *The future we want, Resolution adopted by the General Assembly on 27 July 2012, A/RES/66/288*.

1722 UNGA. (2015). *Transforming our world: the 2030 Agenda for Sustainable Development, Resolution adopted by the*
1723 *General Assembly on 25 September 2015, A/RES/70/1*.

1724 Vanderkelen, I., van Lipzig, N. P. M., Lawrence, D. M., Droppers, B., Golub, M., Gosling, S. N., Janssen, A. B. G.,
1725 Marcé, R., Schmied, H. M., Perroud, M., Pierson, D., Pokhrel, Y., Satoh, Y., Schewe, J., Seneviratne, S. I.,
1726 Stepanenko, V. M., Tan, Z., Woolway, R. I., & Thiery, W. (2020). Global Heat Uptake by Inland Waters.
1727 *Geophysical Research Letters*, 47(12), e2020GL087867. <https://doi.org/10.1029/2020GL087867>

1728 Vasseur, G., Bernard, P., Van de Meulebrouck, J., Kast, Y., & Jolivet, J. (1983). Holocene paleotemperatures
1729 deduced from geothermal measurements. *Palaeogeography, Palaeoclimatology, Palaeoecology*, 43(3–4),
1730 237–259. [https://doi.org/10.1016/0031-0182\(83\)90013-5](https://doi.org/10.1016/0031-0182(83)90013-5)

1731 Verdoya, M., Chiozzi, P., & Pasquale, V. (2007). Thermal log analysis for recognition of ground surface
1732 temperature change and water movements. *Clim. Past*, 3(2), 315–324. <https://doi.org/10.5194/cp-3-315-2007>

1733 von Schuckmann, K., Sallée, J.-B., Chambers, D., Le Traon, P.-Y., Cabanes, C., Gaillard, F., Speich, S., & Hamon,
1734 M. (2014). Consistency of the current global ocean observing systems from an Argo perspective. *Ocean*
1735 *Science*, 10(3), 547–557. <https://doi.org/10.5194/os-10-547-2014>

1736 von Schuckmann, K., & Le Traon, P.-Y. (2011). How well can we derive Global Ocean Indicators from Argo data?
1737 *Ocean Sci.*, 7(6), 783–791. <https://doi.org/10.5194/os-7-783-2011>

1738 von Schuckmann, K., Palmer, M. D., Trenberth, K. E., Cazenave, A., Chambers, D., Champollion, N., Hansen, J.,
1739 Josey, S. A., Loeb, N., Mathieu, P.-P., Meyssignac, B., & Wild, M. (2016). An imperative to monitor Earth's
1740 energy imbalance. *Nature Climate Change*, 6(2), 138–144. <https://doi.org/10.1038/nclimate2876>

1741 von Schuckmann, Karina, Le Traon, P.-Y., Smith, N., Pascual, A., Brasseur, P., Fennel, K., Djevidnia, S., Aaboe, S.,
1742 Fanjul, E. A., Autret, E., Axell, L., Aznar, R., Benincasa, M., Bentamy, A., Boberg, F., Bourdallé-Badie, R.,
1743 Nardelli, B. B., Brando, V. E., Bricaud, C., ... Zuo, H. (2018). Copernicus Marine Service Ocean State
1744 Report. *Journal of Operational Oceanography*, 11(sup1), S1–S142.
1745 <https://doi.org/10.1080/1755876X.2018.1489208>

1746 Wang, G., Cheng, L., Abraham, J., & Li, C. (2018). Consensuses and discrepancies of basin-scale ocean heat
1747 content changes in different ocean analyses. *Climate Dynamics*, 50(7), 2471–2487.
1748 <https://doi.org/10.1007/s00382-017-3751-5>

1749 Wang, X., Key, J., Kwok, R., & Zhang, J. (2016). Comparison of Arctic Sea Ice Thickness from Satellites, Aircraft,
1750 and PIOMAS Data. *Remote Sensing*, 8(9), 713. <https://doi.org/10.3390/rs8090713>

1751 Watts, N., Amann, M., Arnell, N., Ayeb-Karlsson, S., Belesova, K., Boykoff, M., Byass, P., Cai, W., Campbell-
1752 Lendrum, D., Capstick, S., Chambers, J., Dalin, C., Daly, M., Dasandi, N., Davies, M., Drummond, P.,
1753 Dubrow, R., Ebi, K. L., Eckelman, M., ... Montgomery, H. (2019). The 2019 report of The

1754 Lancet Countdown on health and climate change: ensuring that the health of a child born today is
1755 not defined by a changing climate. *The Lancet*, 394(10211), 1836–1878. <https://doi.org/10.1016/S0140->
1756 6736(19)32596-6

1757 WCRP, G. S. L. B. (2018). Global sea-level budget 1993–present. *Earth Syst. Sci. Data*, 10(3), 1551–1590.
1758 <https://doi.org/10.5194/essd-10-1551-2018>

1759 Wijffels, S., Roemmich, D., Monselesan, D., Church, J., & Gilson, J. (2016). Ocean temperatures chronicle the
1760 ongoing warming of Earth. In *Nature Climate Change* (Vol. 6, Issue 2, pp. 116–118). Nature Publishing
1761 Group. <https://doi.org/10.1038/nclimate2924>

1762 Wild, M. (2020). The global energy balance as represented in CMIP6 climate models. *Climate Dynamics*.
1763 <https://doi.org/10.1007/s00382-020-05282-7>

1764 Willis, J. K., Roemmich, D., & Cornuelle, B. (2004). Interannual variability in upper ocean heat content,
1765 temperature, and thermosteric expansion on global scales. *Journal of Geophysical Research: Oceans*,
1766 109(C12). <https://doi.org/10.1029/2003JC002260>

1767 Wilson, N., Straneo, F., & Heimbach, P. (2017). Satellite-derived submarine melt rates and mass balance (2011–
1768 2015) for Greenland’s largest remaining ice tongues. *The Cryosphere*, 11, 2773–2782.
1769 <https://doi.org/10.5194/tc-11-2773-2017>

1770 WMO. (2020). *WMO Statement on the State of the Global Climate in 2019*.
1771 https://library.wmo.int/doc_num.php?explnum_id=10211

1772 Woollings, T., Gregory, J. M., Pinto, J. G., Reyers, M., & Brayshaw, D. J. (2012). Response of the North Atlantic
1773 storm track to climate change shaped by ocean–atmosphere coupling. *Nature Geoscience*, 5(5), 313–317.
1774 <https://doi.org/10.1038/ngeo1438>

1775 Xu, C., McDowell, N. G., Fisher, R. A., Wei, L., Sevanto, S., Christoffersen, B. O., Weng, E., & Middleton, R. S.
1776 (2019). Increasing impacts of extreme droughts on vegetation productivity under climate change. *Nature*
1777 *Climate Change*, 9(12), 948–953. <https://doi.org/10.1038/s41558-019-0630-6>

1778 Yang, H., Lohmann, G., Wei, W., Dima, M., Ionita, M., & Liu, J. (2016). Intensification and poleward shift of
1779 subtropical western boundary currents in a warming climate. *Journal of Geophysical Research: Oceans*,
1780 121(7), 4928–4945. <https://doi.org/10.1002/2015JC011513>

1781 Zanna, L., Khatiwala, S., Gregory, J. M., Ison, J., & Heimbach, P. (2019). Global reconstruction of historical ocean
1782 heat storage and transport. *Proceedings of the National Academy of Sciences*, 116(4), 1126.
1783 <https://doi.org/10.1073/pnas.1808838115>

1784 Zemp, M., Huss, M., Thibert, E., Eckert, N., McNabb, R., Huber, J., Barandun, M., Machguth, H., Nussbaumer, S.
1785 U., Gärtner-Roer, I., Thomson, L., Paul, F., Maussion, F., Kutuzov, S., & Cogley, J. G. (2019). Global glacier
1786 mass changes and their contributions to sea-level rise from 1961 to 2016. *Nature*, 568(7752), 382–386.
1787 <https://doi.org/10.1038/s41586-019-1071-0>

1788 Zhang, J., & Rothrock, D. A. (2003). Modeling Global Sea Ice with a Thickness and Enthalpy Distribution Model in
1789 Generalized Curvilinear Coordinates. *Monthly Weather Review*, 131(5), 845–861.
1790 [https://doi.org/10.1175/1520-0493\(2003\)131<0845:MGSIWA>2.0.CO;2](https://doi.org/10.1175/1520-0493(2003)131<0845:MGSIWA>2.0.CO;2)

1791 Zscheischler, J., Westra, S., van den Hurk, B. J. J. M., Seneviratne, S. I., Ward, P. J., Pitman, A., AghaKouchak, A.,
1792 Bresch, D. N., Leonard, M., Wahl, T., & Zhang, X. (2018). Future climate risk from compound events. *Nature*
1793 *Climate Change*, 8(6), 469–477. <https://doi.org/10.1038/s41558-018-0156-3>

1794